Molecular Therapy
Original Article

# AAV9 Edits Muscle Stem Cells in Normal and Dystrophic Adult Mice

Michael E. Nance,[1] Ruicheng Shi,[2] Chady H. Hakim,[1,3] Nalinda B. Wasala,[1] Yongping Yue,[1] Xiufang Pan,[1] Tracy Zhang,[4,6] Carolyn A. Robinson,[1] Sean X. Duan,[1] Gang Yao,[2] N. Nora Yang,[3] Shi-jie Chen,[5] Kathryn R. Wagner,[4,6] Charles A. Gersbach,[7] and Dongsheng Duan[1,2,8,9]

[1]Department of Molecular Microbiology and Immunology, School of Medicine, University of Missouri, Columbia, MO 65212, USA; [2]Department of Biomedical, Biological and Chemical Engineering, College of Engineering, University of Missouri, Columbia, MO 65212, USA; [3]National Center for Advancing Translational Sciences, NIH, Rockville, MD 20850, USA; [4]The Hugo W. Moser Research Institute, Kennedy Krieger Institute, Baltimore, MD 21205, USA; [5]Department of Physics, University of Missouri, Columbia, MO 65212, USA; [6]Department of Neurology and Neuroscience, Johns Hopkins School of Medicine, Baltimore, MD 21205, USA; [7]Department of Biomedical Engineering, Duke University, Durham, NC 27708, USA; [8]Department of Biomedical Sciences, College of Veterinary Medicine, University of Missouri, Columbia, MO 65211, USA; [9]Department of Neurology, School of Medicine, University of Missouri, Columbia, MO 65212, USA

**CRISPR editing of muscle stem cells (MuSCs) with adeno-associated virus serotype-9 (AAV9) holds promise for sustained gene repair therapy for muscular dystrophies. However, conflicting evidence exists on whether AAV9 transduces MuSCs. To rigorously address this question, we used a muscle graft model. The grafted muscle underwent complete necrosis before regenerating from its MuSCs. We injected AAV9.Cre into Ai14 mice. These mice express tdTomato upon Cre-mediated removal of a floxed stop codon. About 28%–47% and 24%–89% of Pax7$^+$ MuSCs expressed tdTomato in pre-grafts and regenerated grafts ($p > 0.05$), respectively, suggesting AAV9 efficiently transduced MuSCs, and AAV9-edited MuSCs renewed successfully. Robust MuSC transduction was further confirmed by delivering AAV9.Cre to Pax7-ZsGreen-Ai14 mice in which Pax7$^+$ MuSCs are genetically labeled by ZsGreen. Next, we co-injected AAV9.Cas9 and AAV9.gRNA to dystrophic mdx mice to repair the mutated dystrophin gene. CRISPR-treated and untreated muscles were grafted to immune-deficient, dystrophin-null NSG.mdx4cv mice. Grafts regenerated from CRISPR-treated muscle contained the edited genome and yielded 2.7-fold more dystrophin$^+$ cells ($p = 0.015$). Importantly, increased dystrophin expression was not due to enhanced formation of revertant fibers or *de novo* transduction by residual CRISPR vectors in the graft. We conclude that AAV9 effectively transduces MuSCs. AAV9 CRISPR editing of MuSCs may provide enduring therapy.**

## INTRODUCTION

Duchenne muscular dystrophy (DMD) is the most common muscular dystrophy, affecting 1 in 5,000 male births.[1] DMD results from the functional loss of the dystrophin protein, a sub-sarcolemmal protein critical for protecting muscle from contraction-induced injury.[2] In DMD, myofiber degeneration stimulates regeneration from muscle stem cells (MuSCs). As disease progresses, these dystrophin-deficient MuSCs gradually lose regenerative capacity, which eventually leads to muscle wasting and replacement with fibrofatty tissues.[3] Repairing the mutated dystrophin gene in MuSCs holds the promise to not only correct inherent dystrophin deficiency in these cells but also produce dystrophin-positive progeny myofibers that can resist contraction-induced damage.

In the past several years, adeno-associated virus (AAV) delivery of the CRISPR system for genome editing has rapidly advanced gene repair strategies for neuromuscular diseases.[4–6] A series of proof-of-principle studies in various rodent DMD models (such as mdx and mdx4cv mice) and a canine model suggest that AAV delivery of the Cas9 gene and guide RNA (gRNA), two essential components for CRISPR editing, can repair or remove mutations in the dystrophin gene, restore dystrophin expression, and improve muscle and heart function.[5,7–18]

AAV is a versatile family of viral vectors with hundreds of naturally existing and laboratory-engineered capsids that are tailored for different gene therapy applications. Among these, AAV serotype 9 (AAV9) is particularly attractive for DMD gene therapy because it can lead to robust and bodywide muscle transduction in small- and large-animal models for DMD.[19,20] Recent success of systemic AAV9 therapy in spinal muscular atrophy type 1 patients has further raised the hope of clinical translation.[21] In fact, several human trials have been initiated in DMD patients to test systemic AAV9 micro-dystrophin gene replacement therapy.[22,23]

The ability to transduce and edit MuSCs by AAV9 would make this vector highly attractive for CRISPR editing therapy for DMD. Paired-box transcription factor 7-positive (Pax7$^+$) satellite cells are considered the primary contributors for muscle regeneration.[24,25]

Received 27 January 2019; accepted 19 June 2019;
https://doi.org/10.1016/j.ymthe.2019.06.012.

**Correspondence:** Dongsheng Duan, Department of Molecular Microbiology and Immunology, School of Medicine, University of Missouri, M610G Medical Sciences Building, Columbia, MO 65212, USA.
**E-mail:** duand@missouri.edu

Two studies examined AAV9 transduction of satellite cells but reached different conclusions.[9,26] Arnett et al.[26] delivered an AAV9 GFP vector to muscle by direct injection. Despite highly efficient muscle transduction, the authors did not find $Pax7^+$ cells that were also $GFP^+$. Tabebordbar et al.[9] isolated satellite cells from AAV9 CRISPR-treated mice and found that ~4% of $Pax7^+$ cells were edited. It is currently unclear what caused the observed discrepancy. However, technical caveats may provide a plausible explanation. For example, the number of satellite cells that can be analyzed in muscle sections could have limited the ability to detect rarely occurring events. Alternatively, artificial biases can be introduced from *in vitro* manipulation (such as isolation, expansion, and differentiation of myoblasts).

To avoid above-mentioned methodological limitations and reliably determine whether AAV9 can indeed transduce MuSCs in adult mouse muscle, we developed a new approach (M.E. Nance et al., 2018, Mol. Ther., abstract). Specifically, we marked MuSCs with AAV9-mediated delivery of genome-editing tools (either the Cre system or the CRISPR technology). We then grafted AAV9-treated muscle to immune-deficient mice. We found that: (1) the grafted muscle underwent complete necrosis and then regenerated from its own MuSCs with nominal contribution from the host, (2) AAV9 efficiently transduced MuSCs in adult mouse muscle, (3) AAV9-marked MuSCs contributed to muscle regeneration, (4) AAV9-marked MuSCs were successfully renewed in the regenerated graft, (5) AAV9 CRISPR therapy resulted in persistent dystrophin restoration for 18 months in the mdx model for DMD, and (6) the edited genome and repaired dystrophin were successfully detected in grafts regenerated from AAV CRISPR-treated mdx mice. Our studies established AAV9 as a useful tool to genetically mark MuSCs. Importantly, our data suggest that AAV9 CRISPR therapy may provide sustained gene repair therapy for inherited muscle diseases by correcting the mutated gene in MuSCs.

## RESULTS

### Grafted Muscle Underwent Complete Necrosis before Regeneration

To determine whether AAV9 can transduce MuSCs, we used a free muscle graft model. This model has been used to study *de novo* muscle regeneration for more than half a century.[27,28] Specifically, a piece of surgically removed donor muscle is grafted to a host animal. The graft becomes ischemic and undergoes coagulative necrosis soon after transplantation. In the ensuing period, the donor muscle regenerates from MuSCs after clearance of cellular debris and revascularization. To validate this model, we grafted the tibialis anterior (TA) muscle from wild-type mice to the evacuated TA compartment of immune-deficient non-obese diabetic (NOD)-severe combined immunodeficient (SCID)-interleukin 2 receptor common gamma chain null (NSG) mice (Figure 1A). Before grafting, the donor showed normal muscle histology with well-organized myofiber arrays and peripherally localized myonuclei. On immunostaining, these myofibers were dystrophin positive (Figure 1D; Table S1). The graft displayed signs of myonecrosis at day 1 post-transplantation and lost myonuclei by days 2–3 (Figure 1B). Histological features of normal muscle were completely gone in the graft by 1 week after transplantation (Figures 1C and D). At this time, the graft was essentially composed of patchy irregular eosin-stained tissue residuals and inflammatory cells. There were no myonuclei and no dystrophin expression (Figure 1D). By 6 weeks after transplantation, the grafted muscle was regenerated with centrally located myonuclei and sarcolemmal dystrophin expression (Figure 1D).

### Muscle Graft Regeneration Was Primarily Driven by Donor MuSCs

It is generally believed that regeneration derives from donor MuSCs. However, some early studies suggest that host muscle progenitor cells might also contribute significantly to the regeneration of the donor muscle.[29–32]

Our experimental design is based on the assumption that the regenerated muscle mainly originates from donor MuSCs. To clarify this important issue, we performed a cross-transplantation study using adult (2- to 5-month-old) donor and host mice (Figure 2; Table S1). In one set of experiments, we transplanted the TA muscle from NOD.GFP mice to NSG mice (Figures 2A–2C; Figure S1).[33–35] In a separate set of studies, we transplanted the TA muscle from non-obese diabetic (NOD) mice to NSG.GFP mice (Figures 2D–2F).[36,37] In both NOD.GFP and NSG.GFP mice, GFP expression was driven by the ubiquitous CAG promoter. This allowed lineage tracing of GFP-positive cells from NOD.GFP donors and NSG.GFP hosts. Quantification demonstrated that ~97% of myofibers in the regenerated graft were originated from the donor (Figure 2C). In the reciprocal experiment, host contribution accounted for ~3% of myofibers in the graft (Figure 2F).

To assess the extent of host contribution in the context of a dystrophic donor, we transplanted the TA muscle from adult mdx mice to adult NSG and NSG.mdx4cv mice (Figure 2G). NSG mice have normal dystrophin expression, but NSG.mdx4cv mice are dystrophin deficient. On quantification, we found only 0.43% ± 0.10%, 0.16% ± 0.09%, and 0.21% ± 0.08% dystrophin-positive revertant fibers in the TA, extensor digitorum longus, and peroneus longus muscle of NSG.mdx4cv mice, respectively (Figure S2). When the mdx TA muscle was transplanted to the NSG host, we found 1.70% ± 1.84% dystrophin-positive revertant fibers in the regenerated graft (Figure 2H). When the mdx TA muscle was transplanted to the NSG.mdx4cv host, we found 2.65% ± 0.64% dystrophin-positive revertant fibers in the regenerated graft (Figure 2H). If the host has significantly contributed to graft regeneration, we should detect more dystrophin-positive fibers in the muscle grafted to the NSG host. Because there was no statistically significant difference ($p = 0.5333$) in dystrophin-positive cell quantification, we concluded that the host contributed minimally to the regeneration of a dystrophic graft.

To more stringently evaluate host contribution to dystrophic muscle regeneration, we grafted the TA muscle from 19-month-old mdx mice to adult NSG.GFP hosts (Figures 2I–2K). Failure to regenerate is a characteristic feature of the aged dystrophic muscle.[3] It is possible that the diminished regeneration capacity of the aged dystrophic

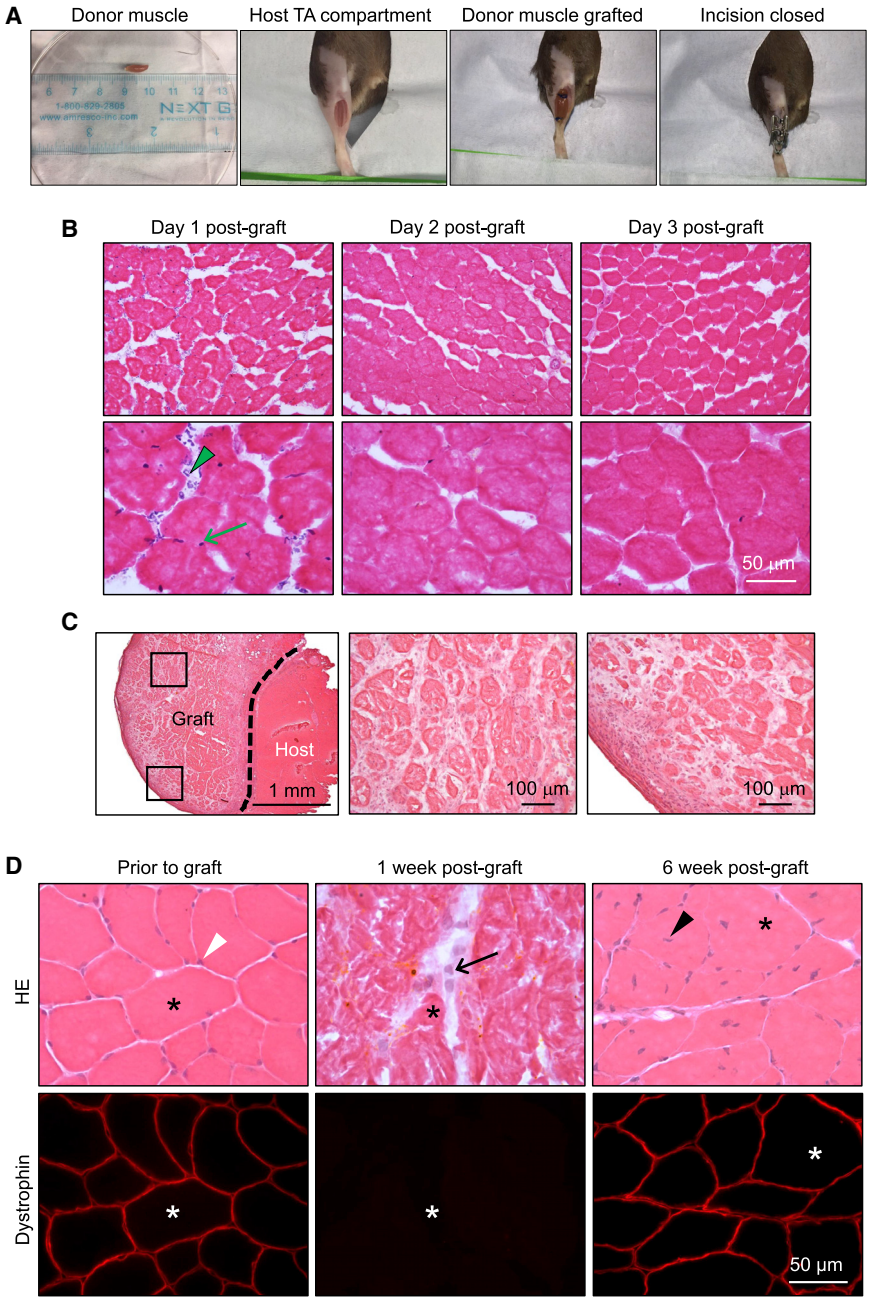


**Figure 1. Establishment of the Free Muscle Graft Model**

(A) Step-by-step illustration of the grafting process. The tibialis anterior (TA) muscle was removed from the donor mouse. The TA compartment in the immune-deficient host mouse was surgically cleared by removing the TA and extensor digitorum longus muscle. The donor TA muscle was sutured to the empty TA compartment of the host mouse. The incision was closed with glue and surgical clamps. (B) Representative H&E staining photomicrographs of a transplanted normal muscle at days 1, 2, and 3 post-grafting (top panels, low-power images; bottom panels, high-power images). Green arrow, myonuclei; green arrowhead, fragmented myonuclei from dying muscle cells. (C) Representative H&E staining photomicrographs of a transplanted normal muscle at 7 days after grafting. Dotted line makes the junction between the graft and the host muscle. High-power images are corresponding boxed areas from the graft. (D) Representative H&E staining and dystrophin immunostaining photomicrograph of the graft before transplantation, 1 week post-transplantation, and after full regeneration (6 weeks post-transplantation). Black arrow, infiltrating inflammatory cells; black arrowhead, centrally localized myonuclei in the regenerated graft; white arrowhead, peripheral localization of myonuclei in the pre-graft; asterisks, the same myofiber in serial sections.

muscle may promote host contribution to graft regeneration. Quantification suggests that the host contributed to only ~0.5% myofibers in the regenerated graft (Figure 2K).

### AAV9.Cre Injection in Ai14 Mice Resulted in Efficient Editing of Pax7$^+$ MuSCs, Robust Regeneration from Edited MuSCs, and Successful Renewal of Edited MuSCs in the Regenerated Muscle Graft

Ai14 mice carry a CAG-LoxP-Stop-LoxP-tdTomato cassette in their genome.[38] In the presence of the Cre recombinase, the LoxP flanked stop codon is removed. This leads to the expression of tdTomato in all edited cells (Figure 3A).

To determine whether AAV9 can transduce Pax7$^+$ MuSCs, we injected AAV9.Cre into Ai14 mouse muscle (Figure 3B; Table S1). Two weeks after AAV9.Cre delivery, we detected robust tdTomato expression in injected muscles, but not in un-injected control muscles (Figure 3C). Pax7 staining was performed to reveal MuSCs (Figure 3D; Figure S1). About 6.6% ± 3.3% of nuclei showed positive Pax7 staining. Among Pax7$^+$ cells, 37.1% ± 13.5% (range: 28%–47%) expressed tdTomato (Figure 3E).

To determine whether AAV9.Cre-edited satellite cells can contribute to muscle regeneration, we grafted the injected muscle to NSG mice (Figure 3B). Small centrally nucleated Pax7$^+$ cells were detected at 7 days after muscle transplantation (Figure 3F). These cells were early-stage regenerating myofibers. Interestingly, some of these cells showed cytoplasmic tdTomato expression, whereas others did not, suggesting both Cre-edited and unedited MuSCs cells have contributed to regeneration (Figures 3F and 3G).

In addition to Pax7$^+$ satellite cells, we also observed tdTomato-positive cells that were morphologically different from satellite cells

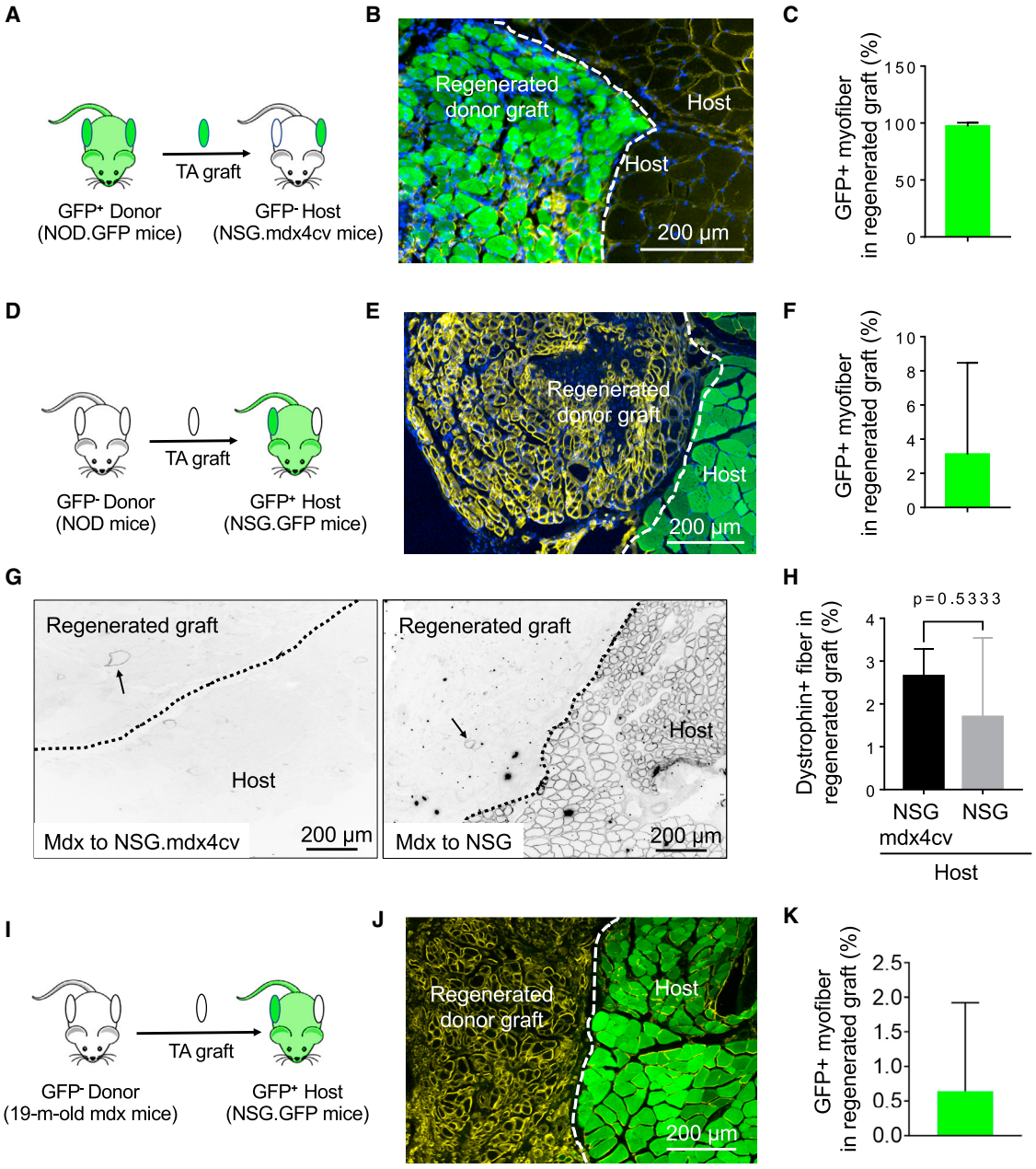


**Figure 2. Donor Muscle Stem Cells Are the Predominant Contributor for Graft Regeneration**

(A) Schematic illustration of grafting GFP$^+$ tibialis anterior (TA) muscle from a NOD.GFP mouse to a NSG mouse. The graft was examined at 6 weeks post-transplantation. (B) A representative immunofluorescence staining photomicrograph demonstrating GFP expression in the regenerated graft muscle (donor), but not in the GFP-negative host muscle. (C) Quantification of GFP$^+$ myofibers in the regenerated muscle graft. (D) Schematic illustration of grafting GFP-negative TA muscle from a NOD mouse to an NSG.GFP mouse. The graft was examined at 6 weeks post-transplantation. (E) A representative immunofluorescence staining photomicrograph demonstrating GFP expression in the host muscle, but not in the regenerated muscle graft. (F) Quantification of GFP$^+$ myofibers in regenerated graft muscle. (G) Representative dystrophin staining photomicrograph following grafting of the mdx tibialis anterior muscle to NSG.mdx4cv mice and NSG mice. Arrows, dystrophin-positive revertant fibers in the regenerated muscle graft. (H) Quantification of dystrophin-positive fibers in the regenerated mdx graft. (I) Schematic illustration of grafting the TA muscle from a 19-month-old mdx mouse to an NSG.GFP mouse. The graft was examined at 6 weeks post-transplantation. (J) A representative immunofluorescence staining photomicrograph demonstrating GFP expression in the host muscle, but not in the regenerated graft. (K) Quantification of GFP$^+$ myofibers in the regenerated graft. In (B), (E), and (J), green color indicates GFP, yellow color indicates laminin, and blue color indicates DAPI. The white dashed line marks the graft-host border.

(Figure S3). These cells stained positive for platelet-derived growth factor receptor alpha (PDGFRα), suggesting they might represent PDGFRα$^+$ mesenchymal stem cells such as fibro-adipogenic progenitors (Figure S3).[39]

At 6 weeks after muscle transplantation, we evaluated the regenerated graft. Robust tdTomato expression was observed in the graft both macroscopically and microscopically (Figures 3H and 3I). On Pax7 immunostaining, 56.9% ± 45.9% (range: 24%–89%) of Pax7$^+$ MuSCs expressed tdTomato (Figure 3J).

### AAV9 Transduction of MuSCs Was Confirmed in Ai14 Mice that Carry Genetically Labeled Pax7$^+$ Cells

To validate the finding in Ai14 mice, we generated Pax7-ZsGreen-Ai14 mice by crossing Ai14 mice with Pax7-ZsGreen mice. In Pax7-ZsGreen mice, an EGFP called ZsGreen is expressed from the Pax7 promoter.[40] This allows identification of Pax7$^+$ MuSCs without using immunostaining. We injected AAV9.Cre to Pax7-ZsGreen-Ai14 mouse muscle (Figure 4A; Table S1). Two weeks after AAV9.Cre delivery, we evaluated ZsGreen and tdTomato expression directly under a fluorescence microscope. Similar to our observations in Ai14 mice, AAV9.Cre injection resulted in robust tdTomato expression in Pax7-ZsGreen-Ai14 mice (Figure 4B). Importantly, 60.3% ± 5.7% of ZsGreen-positive MuSCs expressed tdTomato (Figure 4C).

### One-Time Systemic AAV9 CRISPR Delivery Resulted in Long-Lasting Dystrophin Restoration in Skeletal Muscle

Our studies with AAV9.Cre demonstrated robust transduction of MuSCs by AAV9 and efficient editing of MuSCs by the Cre recombinase. However, the Cre recombinase is a research tool and cannot be used for treating inherited muscle diseases. To determine whether AAV9-mediated MuSC targeting can be capitalized to correct disease-causing mutations in MuSCs, we co-delivered the Cas9 and gRNA vector to 6-week-old mdx mice by tail-vein injection (Figure 5A; Table S1).[8,13] The gRNAs were designed to target introns 22 and 23 of the dystrophin gene. Double-strand breaks were created in introns 22 and 23 by *Streptococcus aureus* Cas9 (SaCas9). The mutated exon 23 was removed from the genome following non-homologous end joining (NHEJ) of the broken ends (Figure 5B).[8] It has been shown that AAV particles can be detected in tissue years after infection.[41,42] We reasoned that prolonged incubation of the AAV vector in muscle *in vivo* might increase the chance of MuSC transduction. Hence, we waited for ~17 months before collecting the TA muscle for grafting. The TA muscle was split in half longitudinally. One part was used to quantify dystrophin expression before grafting, whereas the other part was grafted to NSG.mdx4cv mice. In AAV9 CRISPR-treated mice, we detected 22.4% ± 13.0% dystrophin-positive fibers (Figures 5C and 5D). This was in sharp contrast with age-matched untreated mdx mice in which we found only 1.4% ± 0.5% dystrophin-positive fibers (Figures 5C and 5D). Our results suggest that a single AAV9 CRISPR administration can lead to long-lasting editing of the dystrophin gene in the murine DMD model.[13]

### AAV9 CRISPR Therapy Significantly Increased Dystrophin-Positive Fibers in the Regenerated Graft

Our study in Ai14 mice suggests that AAV-mediated MuSC editing can be studied by grafting an AAV-transduced muscle to an immune-deficient host. To investigate whether AAV9 CRISPR therapy had corrected the mutated dystrophin gene in MuSCs, we grafted AAV9 CRISPR-treated muscles to NSG.mdx4cv host mice. At 6 weeks after grafting, we quantified dystrophin expression in the regenerated graft by immunostaining (Figure 6; Table S1). We detected 4.6% ± 2.7% and 1.7% ± 1.2% dystrophin-positive fibers in grafts regenerated from AAV9 CRISPR-treated and untreated mdx mice, respectively (Figure 6B). The number of dystrophin-positive fibers from the graft of CRISPR-treated mice was significantly higher ($p = 0.015$) (Figure 6B).

We then characterized the distribution pattern of dystrophin-positive myofibers (Figure 6C). Irrespective of prior AAV-9 CRISPR treatment, most dystrophin-positive fibers presented as a single isolated positive myofiber (63.3% ± 12.5% for CRISPR treated and 56.8% ± 32.8% for untreated; $p > 0.05$). Clusters that contained two to four dystrophin-positive fibers constituted 34.6% ± 12.8% and 24.7% ± 20.4% of the positive myofibers in the CRISPR-treated grafts and untreated grafts, respectively ($p > 0.05$). Clusters that had ≥5 dystrophin positive fibers were rarely detected in both groups (2.2% ± 4.7% for CRISPR treated and 1.8% ± 4.5% for untreated; $p > 0.05$) (Figure 6C).

Next, we examined whether the number of dystrophin-positive fibers in pre-grafts correlated with the number in regenerated grafts (Figure 6D). A clear correlation was found in these from untreated mdx mice ($R^2 = 0.8037$). However, no correlation was observed for grafts derived from CRISPR-treated mdx mice ($R^2 = 0.0167$) (Figure 6D).

### Increased Dystrophin Expression Was Not Due to *De Novo* Transduction and Editing of Regenerated Muscle Fibers by Residual CRISPR Vectors in the Graft

To determine whether there was *de novo* transduction and editing of the regenerated muscle, we quantified the AAV vector genome copy number in pre-grafts and regenerated grafts. In the pre-graft, we detected 22.50 ± 9.72 vector genomes per diploid cell (vg/dc) of the SaCas9 vector and 41.70 ± 14.42 vg/dc of the gRNA vector (Figure 7A). In the regenerated graft, we detected 0.05 ± 0.13 vg/dc of the SaCas9 vector and 0.78 ± 0.69 vg/dc of the gRNA vector (Figure 7B).

To determine whether the residual amount of AAV vectors detected in the graft can edit muscle, we co-injected the SaCas9 vector and the gRNA vector to the TA muscle of 10-week-old mdx mice at the doses of 4.65, 46.5, 232.5, 465, and 2,323 vg/dc/vector (Figures 7C–7E; Table S1). Dystrophin-positive myofibers were quantified at 6 weeks after AAV9 injection. In mice that received AAV9 at the doses equal to or lower than 232.5 vg/dc/vector, the percentage of dystrophin-positive cells was identical to that of un-injected control mdx mice

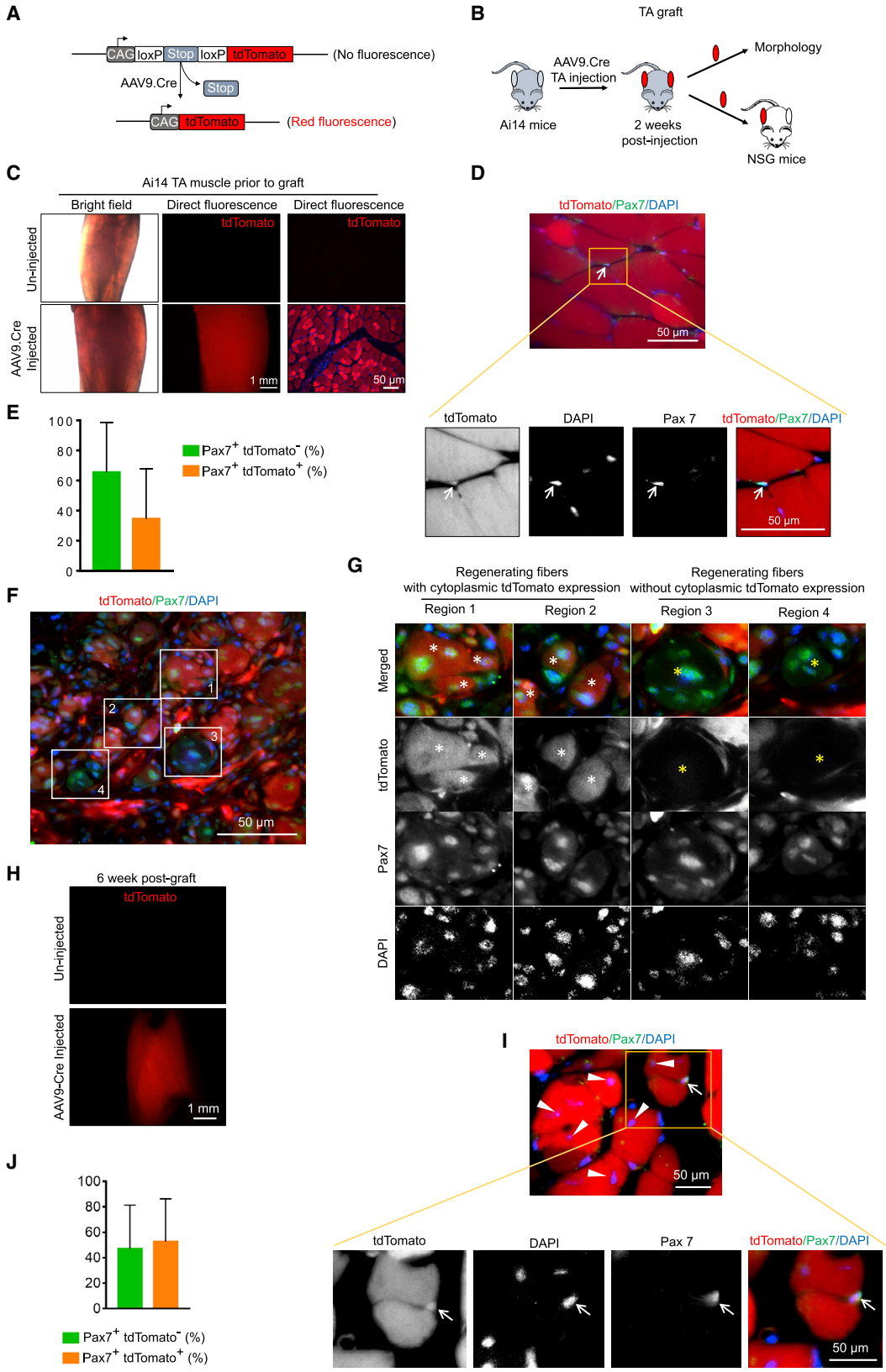


*(legend on next page)*

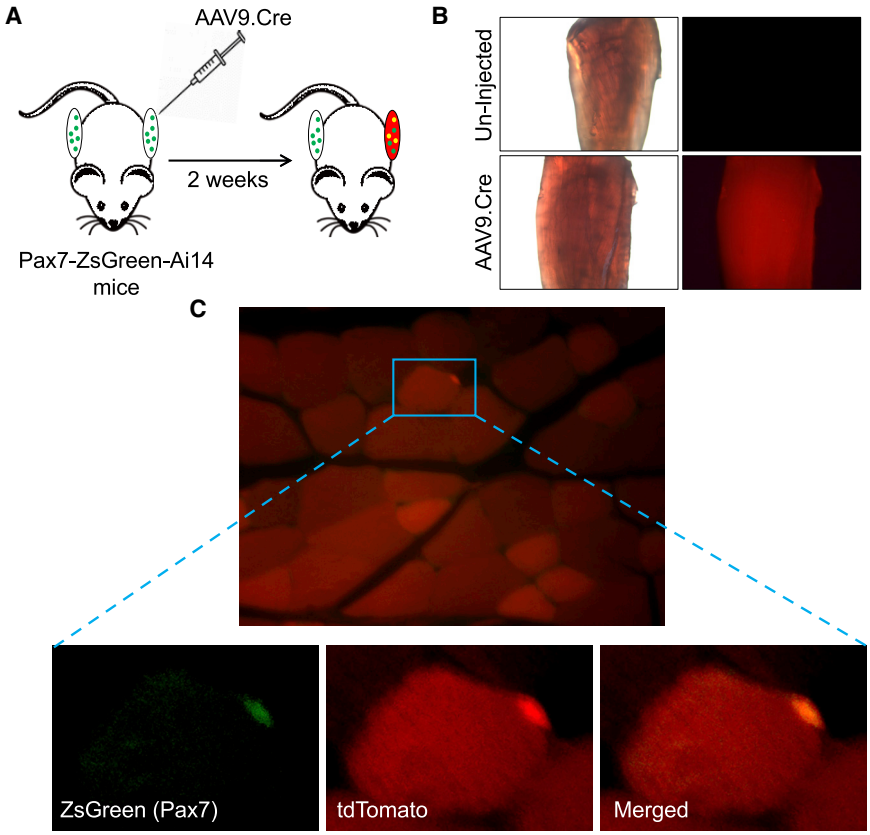


**Figure 4. AAV9 Efficiently Edited Pax7⁺ Muscle Stem Cells in Pax7-ZsGreen-Ai14 Mice**

AAV9-mediated editing of Pax7⁺ muscle stem cells was evaluated by delivering an AAV9.Cre vector to the muscle of Pax7-ZsGreen-Ai14 mice. (A) Schematic illustration of the experimental outline. AAV9.Cre was injected to one side of the tibialis anterior muscle of Pax7-ZsGreen-Ai14 mice. At 2 weeks post-injection, muscle was examined under direct fluorescence microscopy. Green dots, unedited Pax7⁺ muscle stem cells. These cells are genetically marked by ZsGreen. Yellow dots, Pax7⁺ muscle stem cells that are transduced and edited by AAV9.Cre. Red indicates AAV9.Cre injection resulted in saturated expression of tdTomato in muscle. (B) Representative bright-field (left panels) and direct fluorescence (right panels) photomicrographs of the entire TA muscle from uninjected and AAV9.Cre-injected mice. (C) Top panel: a representative direct fluorescence photomicrograph of an AAV9.Cre-injected TA muscle. Bottom panels: a close view of the individual fluorescence channel and the merged images of the boxed region in the top panel. Pax7⁺ muscle stem cells are identified by their inherent ZsGreen expression under direct fluorescence microscopy rather than by indirect immunofluorescence staining.

(Figure 7D). Clearly, the AAV vector genome copy number in pregrafts and regenerated grafts was far from sufficient to transduce and edit regenerated muscle.

### Molecular Evidence for MuSCs Transduction and Genome Editing by AAV9 CRISPR Vectors

The direct evidence for AAV9-mediated MuSC transduction and genome editing is the presence of the modified genome in the regenerated graft. A PCR was designed to detect the edited gene in genomic DNA. The unedited genome should yield a 1.6-kb band, and the edited genome should yield an ~0.47-kb band (Figure 8A). The unedited PCR product was detected in all the samples irrespective of grafting and CRISPR therapy (Figures 8B and 8C). As expected, the edited PCR product was readily detected in the TA muscle from AAV9 CRISPR-treated, but not untreated, mice before grafting (Figure 8B). In regenerated grafts, a faint edited band was detected only in samples

**Figure 3. AAV9 Efficiently Edited Pax7⁺ Muscle Stem Cells in Ai14 Mice**

AAV9-mediated editing of Pax7⁺ muscle stem cells was evaluated by delivering an AAV9.Cre vector to the muscle of Ai14 mice. (A) Schematic illustration of the experimental system. Ai14 mice contain a CAG-loxP-Stop-loxP-tdTomato cassette at the Rosa locus of its genome. AAV9.Cre removes the stop codon and restores tdTomato expression. (B) Experimental outline. AAV9.Cre was injected to both the left and right tibialis anterior (TA) muscle of Ai14 mice. At 2 weeks post-injection, one side of the TA muscle was harvested for morphological studies, and the contralateral TA muscle was grafted to a NSG mouse. (C) Representative bright-field and direct fluorescence photomicrographs of the entire TA muscle. Top panels: a muscle that did not receive AAV9.Cre injection; bottom panels: an AAV9.Cre-injected muscle. Saturated tdTomato expression was seen in only AAV9.Cre-injected TA muscle. (D) Top panel: a representative photomicrograph of an AAV9.Cre-injected TA muscle at 2 weeks after injection. Bottom panels: a close view of the individual fluorescence channel and the merged images of the boxed region in the top panel. Arrows, a Pax7⁺ muscle stem cell that has been transduced and edited by AAV9.Cre. (E) Quantification of Pax7⁺ muscle stem cells expressing (green) or not expressing (gold) tdTomato at 2 weeks after AAV9.Cre injection (before the muscle was grafted). (F) A representative photomicrograph of an AAV9.Cre-treated graft at 1 week post-grafting. Boxes 1 and 2, Pax7⁺ nascent muscle cells with cytoplasmic tdTomato expression; boxes 3 and 4, Pax7⁺ nascent muscle cells without cytoplasmic tdTomato expression. (G) A close view of the boxed regions in (F) demonstrating heterogeneity of tdTomato expression during early regeneration. Regions 1 and 2, newly regenerated muscle cells with Pax7 expression in the nuclei and tdTomato expression in the cytoplasm; regions 3 and 4, newly regenerated muscle cells with Pax7 expression in the nuclei but no tdTomato expression in the cytoplasm. (H) Representative direct fluorescence photomicrographs of the entire graft at 6 weeks post-grafting. Top panel: a graft derived from a muscle not injected with AAV9.Cre; bottom panel: a graft derived from an AAV9.Cre-injected muscle. (I) Top panel: a representative photomicrograph of a fully regenerated graft (6 weeks post-grafting) derived from an AAV9.Cre-injected muscle. Bottom panels: a close view of the individual fluorescence channel and the merged images of the boxed region in the top panel. Arrows, a regenerated Pax7⁺ muscle stem cell that retained tdTomato expression; arrowheads, centrally localized myonuclei. (J) Quantification of Pax7⁺ muscle stem cells expressing (green) or not expressing (gold) tdTomato from fully regenerated grafts that were derived from AAV9.Cre-injected muscle.

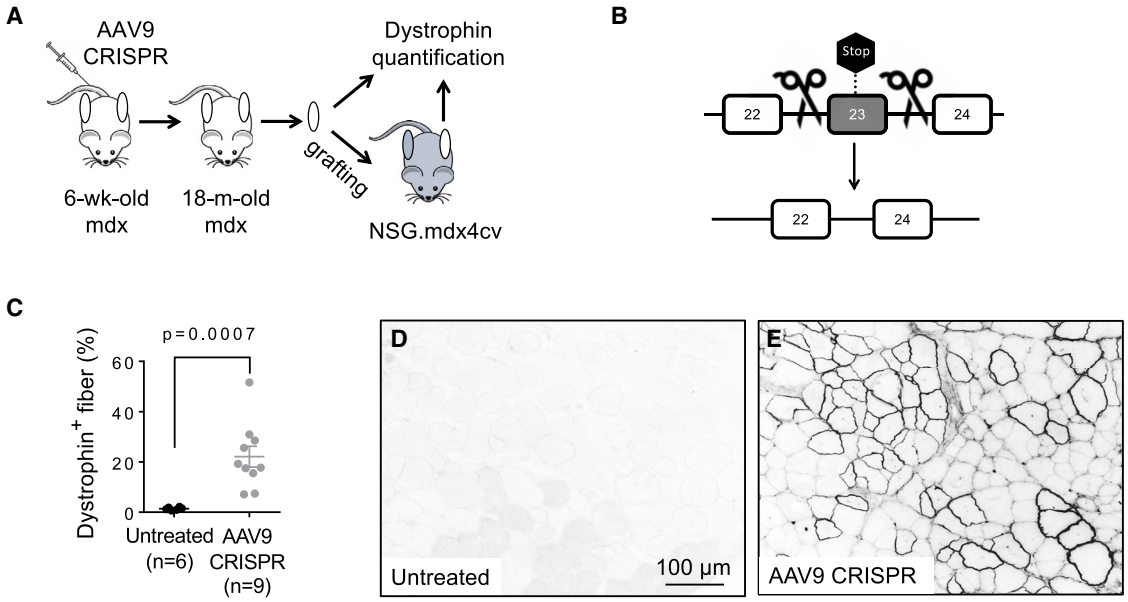


**Figure 5. Systemic AAV9 CRISPR Therapy in Adult mdx Mice Resulted in Long-Lasting Restoration of Dystrophin Expression in the Tibialis Anterior Muscle**
(A) Schematic outline of the experiment. AAV9 CRISPR vectors were delivered to a 6-week-old mdx mouse by tail-vein injection. When the mouse reached 18 months of age, the tibialis anterior muscle was dissected out and split longitudinally in two halves. One half was snap frozen and immunostained for dystrophin. The other half was grafted to a NSG.mdx4cv mouse. (B) Graphic representation of Cas9 and gRNA AAV vectors targeting and cleavage at introns flanking the mutated dystrophin exon 23 (non-sense mutation). In the edited dystrophin gene, exon 23 and its immediate flanking intron regions are removed, and the leftover introns are fused together. (C) Quantification of dystrophin-positive fibers in the tibialis anterior muscle of 18-month-old mdx mice that either did not receive (untreated) or received AAV9 CRISPR therapy at 6 weeks of age. (D) Representative dystrophin staining photomicrographs from an untreated mdx mouse. (E) Representative dystrophin staining photomicrographs from an AAV9 CRISPR-treated mouse.

from CRISPR-treated mice (Figure 8B). To estimate editing efficiency, we quantified the intensity of unedited and edited bands by densitometry (Figure S4). Before grafting, 2.5% ± 1.0% of the mutated dystrophin gene was corrected by AAV9 CRISPR therapy. In the regenerated graft, 0.8% ± 0.3% of the mutated dystrophin gene was corrected (Figure S4).

To further confirm gene editing, we performed nested PCR (Figure 8C). The edited genome should yield an ~0.35-kb band. This band was clearly detected in four out of five regenerated grafts from CRISPR-treated mice (Figure 8C). We cloned and sequenced the smaller band from the nested PCR (Figures 8C and 8D). Before grafting, 11 out of 12 clones showed the expected fusion of intron 22 to 23 as observed previously.[8] The remaining clone had a 1-bp deletion consistent with alternative end processing during NHEJ. In regenerated grafts, 13 out of 14 clones showed expected gene fusion. The remaining clone had a 3-bp deletion (Figure 8D; Figure S5). We also attempted to extract DNA from the corresponding location in grafts from untreated mdx mice. The yield was too low for sequencing.

## DISCUSSION

In this study we established a rigorous and sensitive model system to study MuSC transduction by AAV in adult mice. In this system, AAV-transduced MuSCs are permanently marked by genome editing with the Cre recombinase or Cas9 endonuclease in alive animals. Edited cells are then tracked by *de novo* regeneration in muscle allografts derived from the AAV-treated animals. Using this novel approach, we showed that AAV9 can transduce and edit MuSCs in normal and dystrophic adult mice.

The traditional approach to study AAV tropism is to directly evaluate AAV-mediated reporter gene expression following infection. Using this approach, Arnett et al.[26] showed that AAV9 did not transduce satellite cells. There are several challenges in applying this approach to study AAV transduction in MuSCs. First, myogenic stem cells are extremely rare. For example, satellite cells account for only ~2%–6% of all myonuclei in adult mouse muscle.[43–46] It is technically very demanding to detect transduced satellite cells, especially if only a tiny fraction is transduced. Second, MuSCs have a very small cytoplasmic volume, which makes detection difficult with commonly used reporter genes. Induction of MuSC proliferation should help increase detection sensitivity for a vector that is integrated in the host genome. However, AAV predominantly exists as episomal molecules.[47,48] The vector genome will be diluted during cell division and eventually lost. Third, besides satellite cells, many different non-satellite MuSCs have been reported such as interstitial progenitor cells, side population cells, pericytes, fibro-adipogenic progenitors, and Twist2-dependent progenitor cells.[24,25,49–53] It is very unlikely that a promoter used in one reporter AAV vector is active in all these cells. Hence, only a sub-group (e.g., only satellite cells in the Arnett

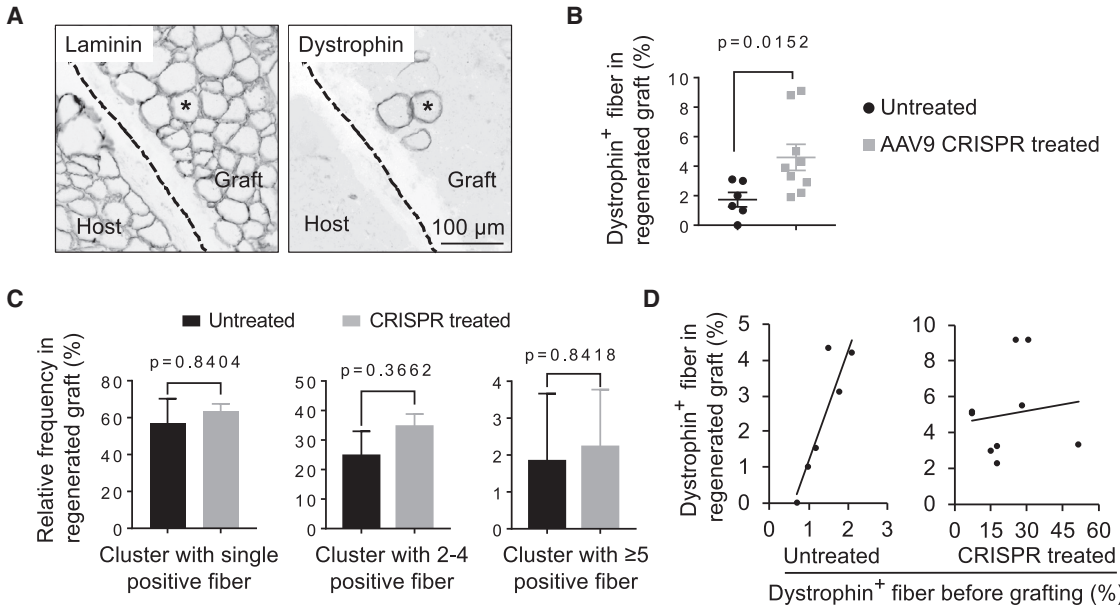


**Figure 6. Quantitative Evaluation of Dystrophin Expression in Regenerated Muscle Grafts**

(A) Representative laminin and dystrophin staining photomicrographs from a graft derived from an AAV9 CRISPR-treated mouse. Asterisks, the same myofiber in series sections. (B) Quantification of dystrophin-positive myofibers in regenerated grafts that originated from mdx mice that either received or did not receive AAV9 CRISPR therapy. (C) Quantification of dystrophin-positive clusters in regenerated grafts. Clusters were grouped as these that had one positive fiber, two to four positive fibers, and five or more positive fibers. (D) Correlation of dystrophin-positive fibers in the same tibialis anterior muscle before grating and after regeneration. Left panel: the donor mdx mice did not receive AAV9 CRISPR therapy; right panel: the donor mdx mice were treated with AAV9 CRISPR therapy at 6 weeks of age.

et al.[26] study), rather than the entire constituent of MuSCs can be studied.

Tabebordbar et al.[9] utilized a different approach. They marked AAV-transduced satellite cells with CRISPR editing and then isolated, cultured, and expanded these cells *in vitro*.[9] The myogenic property was then studied *ex vivo* by forced differentiation or *in vivo* in a muscle injury model.[49,50,53,54] Because the methods used to isolate and expand MuSCs are often optimized for a particular type of MuSCs (e.g., for satellite cells in the Tabebordbar et al.[9] study), similar to the Arnett et al.[26] study, this approach also cannot study the entire pool of MuSCs. Importantly, data can be confounded by the inevitable biases from *in vitro* manipulation, such as incomplete and/or incorrect labeling of MuSCs with antibodies used in flow cytometry, loss of MuSCs during cell isolation, and survival of injected MuSCs in the host animal muscle.

To minimize technical and/or biological concerns of the reporter vector and cell culture-based approaches, we studied AAV9 tropism in MuSCs by combining genetic marking and muscle grafting (Figures 1, 2, 3, 4, 5, and 6). Compared with the methods used in previous studies,[9,26] our approach has several advantages. First, transduced and edited MuSCs can be permanently labeled and tracked. Second, the entire myogenic cell population, instead of a particular type, can be studied in the original extracellular matrices of the donor muscle without *ex vivo* handling steps (e.g., purification, labeling, culture, and injection). Third, detection sensitivity is significantly improved by the proliferation and regeneration of the AAV-transduced and edited MuSCs. Fourth, self-renewal of the genetically modified MuSCs can be investigated. This last point is especially worth noting because self-renewal of edited MuSCs cannot be studied with any existing methods.

To examine AAV9 transduction of MuSCs with our new approach, we started with the Cre system, a widely used experimental tool to edit genes that have been floxed. We delivered AAV9.Cre to Ai14 mice by intramuscular injection (Figure 3). Ai14 mice contain a floxed stop cassette that blocks tdTomato expression.[38] The Cre recombinase expressed from AAV9 should remove the stop cassette and result in permanent marking of AAV9-transduced cells as tdTomato-positive cells (Figure 3A). Two weeks following AAV9.Cre injection, we observed saturated tdTomato expression throughout the entire muscle, suggesting efficient transduction and editing of mature myonuclei (Figure 3C). Importantly, tdTomato expression was detected in approximately one-third to one-half of $Pax7^+$ satellite cells (Figures 3D and 3E). After grafting, we detected regeneration of $Pax7^+$ satellite cells that are either transduced and edited or not transduced and edited by AAV9 (Figures 3F and 3G). The progeny from edited satellite cells expressed tdTomato in the cytoplasm (regions 1 and 2 in Figures 3F and 3G). The progeny from unedited satellite cells had no cytoplasmic tdTomato expression (regions 3 and 4 in Figures 3F and 3G). Nevertheless, tdTomato expression was detected in every myofiber in the fully regenerated graft because of the fusion of $tdTomato^+$ and $tdTomato^-$ progeny muscle cells (Figures 3H and 3I).

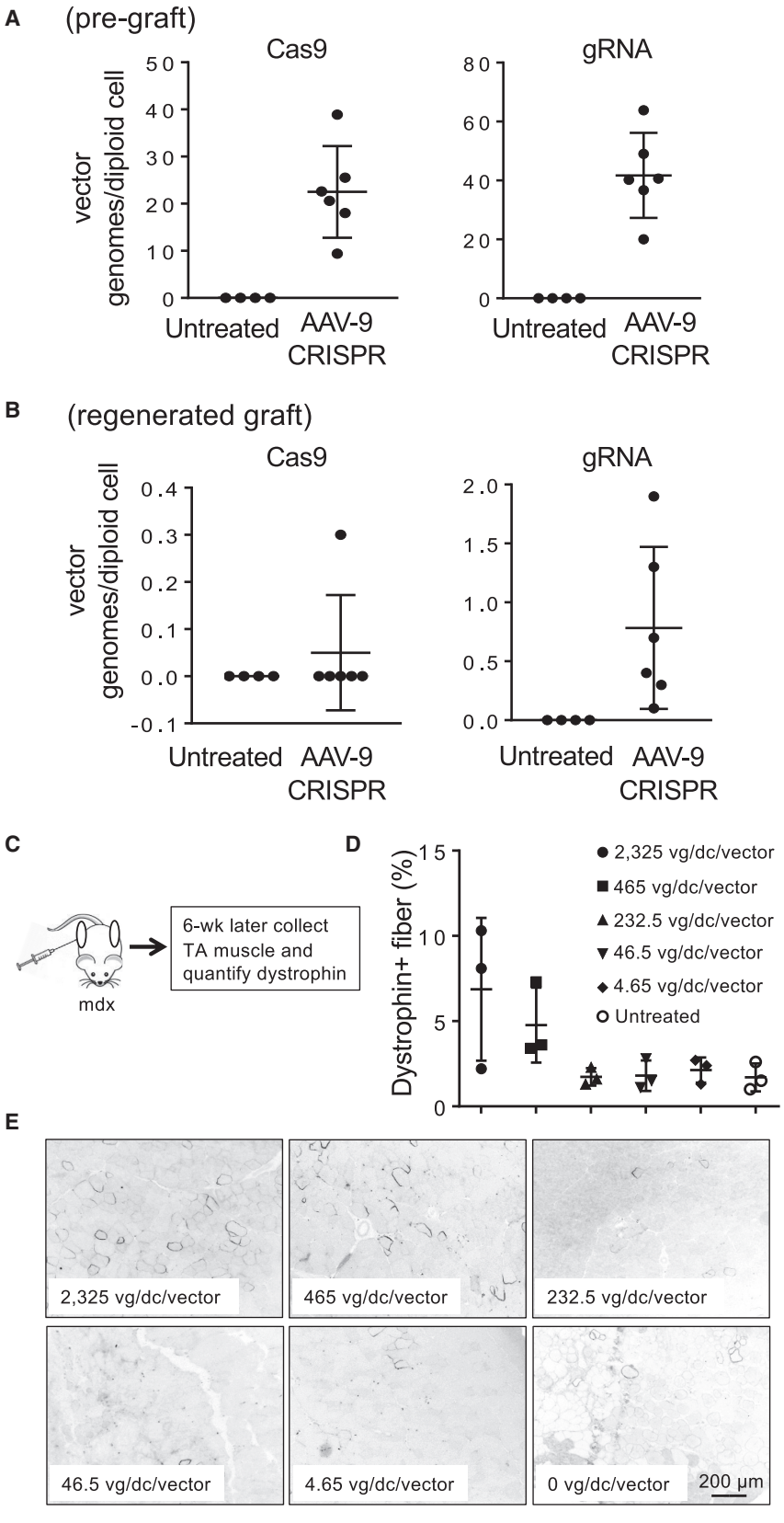


**Figure 7. The Residual gRNA and SaCas9 Vector Genomes in the Pre- and Post-graft Muscle Are Insufficient for *De Novo* Genome Editing**

(A) Results from the TaqMan PCR assay detecting SaCas9 (left panel) and gRNA (right panel) vector genomes for untreated (n = 4) and CRISPR-treated (n = 6) in pre-graft. (B) Results from the TaqMan PCR assay detecting SaCas9 (left panel) and gRNA (right panel) vector genomes for untreated (n = 4) and CRISPR-treated (n = 6) in regenerated grafts. (C) Schematic illustration of the experimental design for the local injection study. Various doses of gRNA and SaCas9 vectors were injected to the tibialis anterior muscle of 6-week-old mdx mice, and the muscle was collected 6 weeks later for analysis. (D) Quantitation of dystrophin expression as a function of the injected vector dosage (n = 3/dose). (E) Representative dystrophin immunostaining images from each local injection dose group as in (D) are shown with the corresponding vg/dc/vector (vector genome/diploid cell/vector) value.

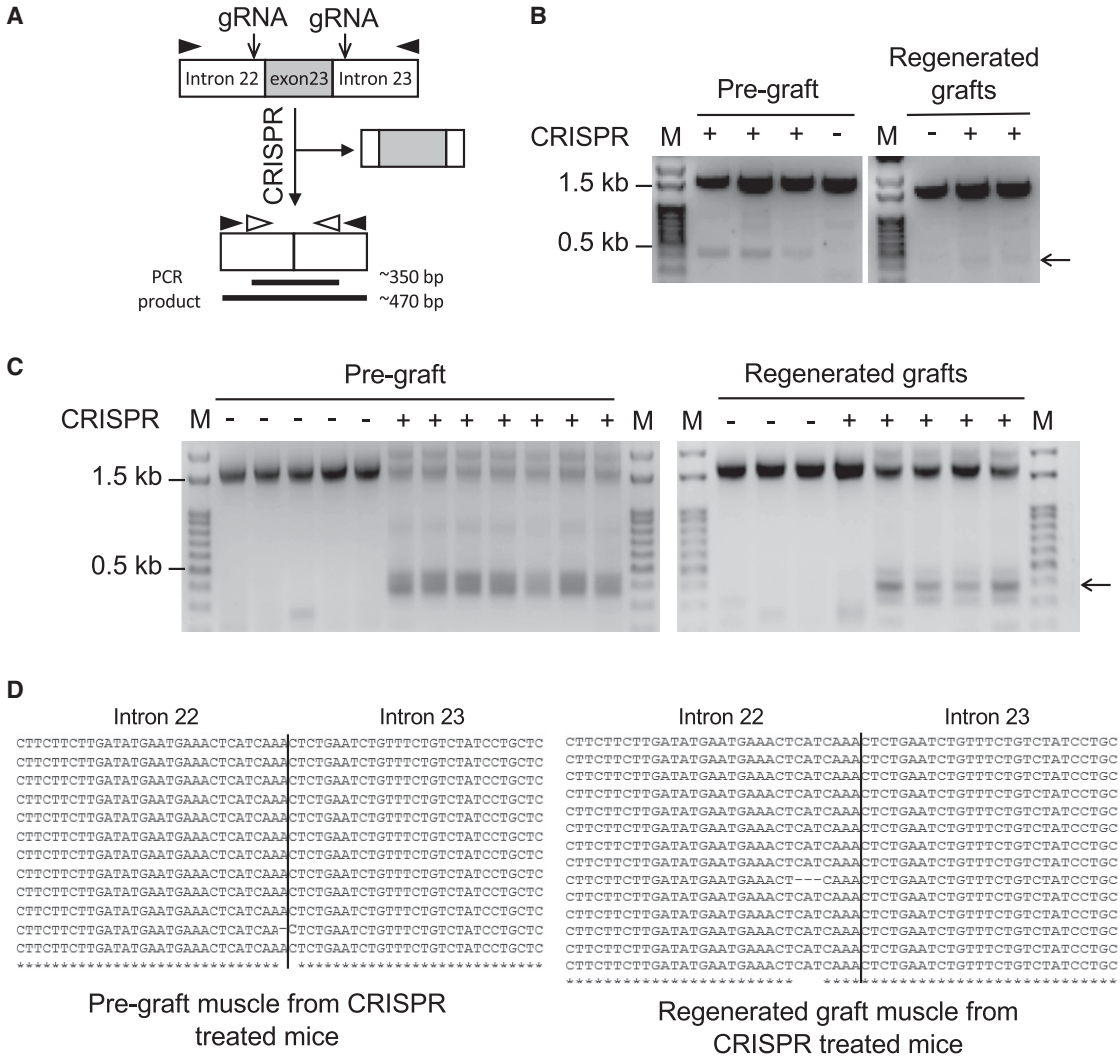


**Figure 8. Molecular Demonstration of AAV9-Mediated CRISPR Editing in Myogenic Progenitor Cells**

(A) Schematic illustration of the PCR used in the experiment. Two gRNAs were designed to direct the Cas9 endonuclease to make double-strand breaks in intron sequences flanking exon 23. Exon 23 and flanking intron sequences were removed. The broken ends were ligated through non-homologous end-joining. Black arrowheads, location of the primers used in the PCR shown in (B); white arrowheads, location of the primers used in the nested PCR shown in (C). (B) Representative agarose gel photomicrographs of the PCR results using primers marked as black arrowheads in (A). In the unedited genome, this PCR yielded a 1.6-kb product. In the edited genome, this PCR yielded a ~470-bp product. Left panel: the edited band was detected only in donor muscle originating from AAV9 CRISPR-treated mice. Right panel: a faint edited band was detected in regenerated grafts that were originated from AAV9 CRISPR-treated mice. Arrow, edited band. (C) Representative agarose gel photomicrographs of the nested PCR results using primers marked as white arrowheads in (A). The nested PCR was performed by addition of the nested PCR primers to one-fifth of the first-round PCR products. Due to the presence of both the nested primers and first-round PCR primers, both unedited (1.6 kb) and edited genome (~350–~470 bp) can be detected. No edited band was detected in donor muscle derived from untreated mdx mice. The edited band was detected in all pre-graft muscle samples from mice that have received CRISPR therapy. In regenerated grafts originating from CRISPR-treated mice, the edited band was detected in all except one sample. Arrow, edited band. For (B) and (C), each lane represents an independent muscle sample. (D) Sequence alignment at the expected intron 22 and 23 junction in the edited genome. Left panel: results from 12 randomly selected clones of pre-graft muscles; right panel: results from 14 randomly selected clones of regenerated grafts. M, molecular weight marker.

A salient feature of muscle regeneration is asymmetric division of satellite cells.[3] This leads to the replenishment of the satellite cell pool for future regeneration. If AAV9-edited satellite cells were successfully renewed, we should see Pax7 and tdTomato double-positive satellite cells in the regenerated graft. Indeed, nearly half of $Pax7^{+}$ satellite cells expressed tdTomato in the regenerated graft (Figures 3I and 3J). This piece of data demonstrated for the first time that AAV9-edited MuSCs are capable of self-renewal. These renewed MuSCs may then contribute to regeneration in the future.

To completely exclude artifacts from experimental manipulations (such as these caused by low specificity of the antibody used in

immunostaining), we generated a new strain of Ai14 mice in which $Pax7^+$ cells were genetically marked with ZsGreen (Figure 4). Similar to what we saw in the original Ai14 mice, we observed robust tdTomato expression in the muscle of Pax7-ZsGreen-Ai14 mice after AAV9.Cre injection (Figures 4B and 4C). Under direct fluorescence microscopy, we tracked AAV9 transduction of MuSCs. On quantification, ~60% of ZsGreen-positive satellite cells were also tdTomato positive. Collectively, our results from Ai14 mice and Pax7-ZsGreen-Ai14 mice suggest that $Pax7^+$ MuSCs can be efficiently transduced by AAV9. Further, the genome of $Pax7^+$ MuSCs can be readily edited by Cre recombinase.

The ultimate goal of our study is to develop MuSC editing as an effective gene repair modality to treat inherited muscle diseases such as DMD. To this end, we packaged a proven CRISPR editing system in AAV9 and injected to young adult mdx mice intravenously. This system is composed of a SaCas9 vector and a gRNA vector. It can efficiently remove the mutated exon 23 in the dystrophin gene and restore dystrophin expression in mdx mice (Figure 5B).[8,13] At ~17 months after AAV9 injection, we grafted muscles from CRISPR-treated and untreated mice to NSG.mdx4cv mice (Figure 5A). Six weeks later, we evaluated the regenerated graft by immunostaining and PCR for dystrophin-positive cells and the edited genome, respectively. By dystrophin staining, we found 2.7-fold more dystrophin-positive myofibers in the graft regenerated from AAV9 CRISPR-treated mice relative to the graft from age-matched untreated mice ($p = 0.0152$) (Figure 6B). By PCR, we detected the edited dystrophin gene only in grafts regenerated from AAV9-treated mice (Figures 8A–8C). These results suggest that AAV9 CRISPR vectors have transduced and edited MuSCs.

To further substantiate our conclusion, we performed extensive control experiments to thoroughly rule out all other possibilities. Theoretically, dystrophin-positive cells seen in regenerated grafts can come from the host and/or the donor. To determine the extent of host contribution, we first conducted a reciprocal transplantation study with $GFP^+$ donor-$GFP^-$ host and $GFP^-$ donor-$GFP^+$ host pairs in normal mice (Figures 2A–2F). The GFP signal is genetically marked in all cells in GFP-positive mice (including progeny derived from stem cells of these mice). By tracking GFP expression in the regenerated graft, we reached the conclusion that contribution from the host was nominal (~3%) (Figures 2A–2F). Next, we grafted young adult mdx muscle to either normal or dystrophic hosts. Again, we did not detect a meaningful contribution of the host (<3%) (Figures 2G and 2H). Because we transplanted the CRISPR-treated mouse muscle at 18 months after AAV9 injection, we next examined whether the donor age could make a difference. The muscle from 19-month-old mdx mice was grafted to a GFP-positive normal host. In the regenerated graft, we barely detected any contribution from the host (~0.5%) (Figures 2I–2K). Collectively, these control experiments provided unequivocal evidence that the host contributed minimally to graft regeneration.

To completely exclude host contribution in our study, we intentionally used NSG.mdx4cv mice as the host. These mice had less than 0.5% dystrophin-positive revertant fibers (Figure S2).[55] Because the host can contribute only 3% at the most (Figure 2), the maximum number of dystrophin-positive cells that NSG.mdx4cv mice can contribute to the regenerated graft would be 0.015%. This is far too low to have any significant impact on our study.

The donor contribution could come from: (1) carry-over of dystrophin-positive myofibers from the pre-graft, (2) *de novo* transduction of regenerated muscle by residual AAV vectors in the graft, (3) revertant fibers, and (4) regeneration from AAV9 CRISPR-edited mdx MuSCs. We excluded the first possibility because none of the dystrophin-positive cells in the donor muscle can survive through the necrotic process after grafting (Figure 1D). To determine whether the residual AAV vector could make a difference, we quantified the copy number of the gRNA and Cas9 vector genomes in the pre-graft and regenerated graft (Figure 7). The AAV copy number in the pre-graft was less than 40 and 60 vg/dc for the Cas9 and gRNA vector genome, respectively (Figure 7A). AAV genomes in regenerated grafts were less than 0.3 and 1.8 vg/dc for the Cas9 and gRNA vector genome, respectively (Figure 7B). These numbers are significantly below the threshold required for effective transduction and gene editing (>232.5 vg/dc) (Figures 7C–7E).

Revertant fibers are rarely occurring dystrophin-positive cells in dystrophic muscle.[56] The ability to generate revertant fibers is an inherent property of a sub-population of myogenic progenitor cells in mdx muscle.[57] These cells have a yet poorly understood but inheritable epigenetic mechanism that restores the open reading frame by alternative splicing.[57,58] To monitor the contribution of revertant fibers, we grafted the age-matched untreated mdx TA muscle. There were 1.4% ± 0.7% of revertant fibers in the pre-graft (Figure 5C) and 1.7% ± 1.2% in the regenerated graft ($p > 0.05$) (Figure 6B). Clearly, the grafting process per se did not promote revertant fiber formation. It is worth noting that dystrophin-positive revertant fibers never exceeded 3% in any graft regenerated from untreated control muscle, whereas the average of dystrophin-positive cells in the graft regenerated from AAV9-treated muscle reached 4.6% (Figure 6B). Hence, a sub-population of dystrophin-positive cells seen in the AAV9-treated graft must have come from transduced and edited MuSCs. To further exclude the revertant fibers as the sole contributor of dystrophin-positive fibers in the graft regenerated from AAV9-treated muscle, we studied the correlation of dystrophin-positive cells in the pre-graft and the regenerated graft. Because revertant fibers originate from a unique population of inherently marked stem cells,[57,58] the number of revertant fiber count before grafting should correlate well with that after regeneration for the same muscle. We observed an excellent correlation in grafts derived from untreated, but not AAV9-treated, mice (Figure 6D). This piece of evidence further supports the notion that AAV9 CRISPR vectors have transduced and edited MuSCs.

Our data suggest that transduction of MuSCs by AAV9 is responsible for the nearly tripled number of dystrophin-positive cells in grafts regenerated from CRISPR-treated mice (Figure 6B). To further

corroborate our reasoning, we quantified the distribution pattern of dystrophin-positive cells in the regenerated graft. There was no significant difference in the cluster formation between grafts regenerated from untreated and CRISPR-treated mice (Figure 6C). For grafts derived from untreated mdx mice, the distribution pattern reflects the behavior of a special group of epigenetically imprinted MuSCs.[57,58] Similarly, for grafts derived from CRISPR-treated mdx mice, the distribution pattern reflects the behavior of the edited MuSCs.

To seek genetic evidence for MuSCs transduction and editing by AAV9, we examined the pre-graft and regenerated graft for the modified genome (Figure 8). By PCR and sequencing analysis, we detected the edited dystrophin gene only in grafts from AAV9 CRISPR-treated mice. By Sanger sequencing, we found precise ligation of the predicted cut site in the gRNA target sites in 11 out of 12 clones obtained from the pre-graft. Consistent with the finding in the pre-graft, we also detected precise ligation in 13 out of 14 clones in the regenerated graft (Figure 8D; Figure S5).

In this study, we have used two different gene-editing methods to permanently mark AAV9-transduced MuSCs. Using the Cre method, we observed highly efficient MuSC transduction by AAV9, reaching ~30%–60% (Figures 3 and 4). However, in our CRISPR study, we merely detected 4.6% of dystrophin-positive myofibers in the regenerated graft (Figure 6). Although extensive future studies are needed to fully address the observed discrepancy, we suspect that it may likely be because of the differences in the experimental setting such as the delivery route, vector dose, gene-editing mechanism, health status of the muscle, and the promoter that was used to drive expression.

The delivery route and vector dose are two known factors that affect AAV transduction *in vivo*. In the Cre study, AAV9 was directly injected into the muscle. The injected viral vectors can immediately start transducing muscle. In the CRISPR study, AAV9 was delivered via the tail vein. AAV9 vectors have to get out from the vasculature before they can transduce muscle.[19] In the Cre study, $1 \times 10^{11}$ vg AAV particles were delivered to a single TA muscle (~40 mg). This is equal to a dose of $\sim 2.5 \times 10^{9}$ vg/mg. In the CRISPR study, $1 \times 10^{13}$ vg of the Cas9 vector and $3 \times 10^{13}$ vg of the gRNA vector were co-injected to an adult mdx mouse (~25 g) via the tail vein. This is equal to a dose of $\sim 0.4 \times 10^{9}$ vg/mg for the Cas9 vector and $\sim 1.2 \times 10^{9}$ vg/mg for the gRNA vector. The necessity to have to overcome the vascular barrier and the lower relative vector dose might have at least partially contributed to the low efficiency observed in the CRISPR study.

The difference in the editing mechanisms between the Cre system and the CRISPR system may have also played a role. For Cre editing to occur, all that is required is to express the Cre recombinase from a single AAV vector. The Cre recombinase then catalyzes recombination between two identical LoxP sites. For CRISPR editing, gene editing requires co-delivery of two different AAV vectors (AAV9.Cas9 and AAV9.gRNA). Further, we have to cut the genome at two different locations that share minimal homology and have different cutting efficiency (Figure 5B). Cutting at one location is not sufficient to restore dystrophin expression. Hence, the CRISPR editing strategy used in this study is inherently more challenging than that of the Cre editing strategy.

Cellular microenvironment has also been shown to profoundly influence AAV transduction efficiency. The Cre study was performed in normal mice, whereas the CRISPR study was performed in dystrophic mice. The ongoing degeneration and regeneration, inflammation, and fibrosis in mdx mice may positively or negatively influence MuSC transduction by AAV9 and subsequent genome editing. Last, but not least, the poor editing in the CRISPR study may be at least partially accounted for by the promoter use. In the Cre study, Cre and tdTomato were expressed from the CB and CAG promoter, respectively. The CB promoter drives robust expression in mouse stem cells.[59] The CAG promoter is a potent promoter in $Pax7^{+}$ MuSCs.[60] In the CRISPR study, Cas9 was expressed from the cytomegalovirus (CMV) promoter, a promoter that is known to have poor activity in stem cells.[59]

In summary, by combining muscle grafting with two different genetic marking technologies (CRISPR and Cre), we demonstrated that AAV9 can transduce MuSCs in adult mice by local or systemic delivery in three independent animal models (Ai14 mice, Pax7-ZsGreen-Ai14 mice, and mdx mice). The finding from systemic delivery in mdx mice is especially significant. With further optimization of the editing machinery and/or gene delivery strategy (such as the expression of Cas9 from a promoter that is highly active in MuSCs, the use of the single gRNA editing approach, the package of Cas9 and gRNA in a single AAV vector, and the delivery of CRISPR components with alternative AAV capsids that are more potent in transducing MuSCs), it is very likely that AAV-based MuSC editing may one day be used to treat human patients.

## MATERIALS AND METHODS

### Experimental Animals

All animal experiments were approved by the institutional animal care and use committee and were in accordance with NIH guidelines. The strain, age, and sample size of experimental mice are summarized in Table S1. BL10 (C57BL/10ScSnJ, stock number 000476), Mdx (C57BL/10ScSn-*Dmd*$^{mdx}$/J, stock number 0001801), mdx4cv (B6Ros.Cg-Dmdmdx-4Cv/J, stock No. 002378), NOD (NOD/ShiLtJ, stock No. 001976), NOD.GFP [NOD.FVB-Tg(CAG-luc,-GFP) L2G85Chco/FathJ, stock No. 010542], NSG (NOD.Cg-Prkdcscid Il2rgtm1Wjl/SzJ, stock No. 005557), NSG.GFP [NOD.Cg-Prkdcscid Il2rgtm1Wjl Tg(CAG-EGFP)1Osb/SzJ, stock No. 021937], and Ai14 [B6;129S6-*Gt(ROSA)26Sor*$^{tm14(CAG-tdTomato)Hze}$/J, stock No. 007908] mice were originally purchased from The Jackson Laboratory (Bar Harbor, ME, USA).[33–38,61,62] NSG.mdx4cv mice and Pax7-ZsGreen mice were generously provided by Dr. Michael Kyba (University of Minnesota) (notably, Pax7-ZsGreen mice are now also available from The Jackson Laboratory; https://www.jax.org/strain/029549).[40,63] All experimental mice were generated in a specific

pathogen-free barrier facility using breeders from The Jackson Laboratory or Dr. Michael Kyba's laboratory.

A new mouse strain we named Pax7-ZsGreen-Ai14 mice was specifically generated for this study. Pax7-ZsGreen-Ai14 mice were Ai14 homozygous and Pax7-ZsGreen heterozygous. These mice were generated in two steps. First, we generated Pax7-ZsGreen heterozygous and Ai14 heterozygous mice by crossing Ai14 mice with Pax7-ZsGreen mice. Next, we crossed Pax7-ZsGreen/Ai14 double-heterozygous mice with Ai14 homozygous mice. Pax7-ZsGreen-Ai14 mice were identified by PCR using protocols described at The Jackson Laboratory website (https://www.jax.org/jax-mice-and-services/customer-support/technical-support/genotyping-resources). All experimental mice were maintained in a specific pathogen-free animal care facility on a 12-h light (25 lux) and 12-h dark cycle with access to food and water *ad libitum*. Unless specified, both male and female mice were used in the study.

### Recombinant AAV9 Vector Production, Purification, and Delivery

The *cis* plasmids pCre, pTRSaCas9, and pTRgRNAs were published before.[8,64] The pCre plasmid is a generous gift of Dr. Weidong Xiao (Temple University).[64] In pCre, the Cre recombinase gene was expressed from the CB promoter.[64,65] In pTRSaCas9, the *Staphylococcus aureus* Cas9 cDNA was expressed from the CMV promoter. In pTRgRNAs, the gRNAs targeting introns 22 and 23 were expressed from the U6 promoter. The AAV9 packaging plasmid was a generous gift of Dr. James Wilson (University of Pennsylvania).[66] The AAV was packaged in AAV9 using the triple-plasmid transient transfection method and purified through three rounds of cesium chloride ultracentrifugation according to our published protocol.[67] Viral titer was determined using the Fast SYBR Green Master Mix kit (Bio-Rad, Hercules, CA, USA) by quantitative real-time PCR in an ABI 7900 HT qPCR machine (Applied Biosystems, Foster City, CA, USA). For AAV9.Cre local injection experiments, $1 \times 10^{11}$ vg particles of AAV were injected to a TA muscle in a final volume of 50 μL using a 31G Hamilton syringe (Figures 2 and 3). For systemic delivery of the CRISPR vectors (Figure 5), AAV was delivered through the tail vein over a period of 60 s in a final volume of 500 μL/mouse at the dose of $1 \times 10^{13}$ vg/mouse for the SaCas9 vector and $3 \times 10^{13}$ vg/mouse for the gRNA vector. For local injection of the CRISPR vectors, various doses of gRNA and SaCas9 vector (Figures 7C–7E) were combined in a final volume of 50 μL and injected into the TA muscle using a 31G Hamilton syringe.

### Total TA Myonuclei Estimation

For local muscle injection, the AAV dose (vg/dc) was determined by dividing the total amount of vg particles delivered per muscle with the total myonuclei number in the TA muscle. To calculate the total myonuclei number in the TA muscle, we first calculate the total myonuclei number in a single myofiber by multiplying the myonuclei density (number of myonuclei per mm length) with the fiber length (mm) according to published data. Specifically, the myonuclei density was reported to range from 30 to 77 nuclei/mm.[68,69] The TA muscle fiber length was reported to range from 5.28 ± 0.96 to 7.2 ± 0.2 mm with the longest length being 7.4 mm.[70–72] In our calculation, we used the high-end number for both the myonuclei density (77 nuclei/mm) and the myofiber length (7.4 mm). The total myonuclei number in the TA muscle was calculated by multiplying the total myonuclei number per myofiber with the total myofiber number in the TA muscle. The average number of fibers per TA cross-section was 1,790 ± 380. This calculation yielded 1,075,074 nuclei per TA muscle. This number was subsequently used to determine the quotient for each dose of vector genomes (Figures 7D and 7E).

### Free Muscle Graft

All of the materials and instruments used in surgery were sterilized either by autoclave or gas sterilization. Mice were given 3 μg/g body weight Banamine subcutaneously for pre-operative pain management. Anesthesia was induced with 3%–5% isoflurane and maintained with 1%–2% isoflurane. The hair from the hind limbs was removed with Nair. The skin was prepped with chlorhexidine solution and then allowed to air-dry. The TA muscle from the donor mouse was carefully dissected out under sterile condition and stored in muscle graft media (DMEM with high glucose, 10% fetal bovine serum, 110 mg/mL sodium pyruvate, and 1% penicillin and streptomycin) on ice.

Free muscle grafts were performed according to our published protocol (Figure 1A).[73] In brief, a single vertical incision was made extending from the knee to the ankle overlying the TA muscle. The fascia covering the TA muscle was removed carefully to avoid damaging any neurovasculature. The distal tendon of the TA muscle was cut and the muscle was resected. The distal tendon of the EDL muscle was then identified, cut, and reflected. The proximal attachments of the TA and EDL muscles were cut following the contours of the tibia, and the entire muscles were removed. The proximal and distal tendons of the peroneus longus muscle were identified. A suture loop was placed around the tendon at these locations using a 4-0 polypropylene suture. The donor muscle was then placed into the empty TA compartment and sutured into place using the loops attached to the adjacent peroneus longus muscle. No neurorrhaphy or reanastomosis was performed. The skin overlying the muscle was closed with surgical glue and staples. Anesthesia was discontinued, and the mouse was observed until awake and moving. Mice were given 3 μg/g body weight Banamine subcutaneously for post-operative pain management.

### Tissue Harvest and Morphology Studies

Mice were euthanized at the end of the study, and muscle tissues were carefully dissected out and flash frozen in optimal cutting temperature compound (OCT) (Sakura Finetek, Torrance, CA, USA) in liquid nitrogen-cooled isopentane and then stored at −80°C until use. Ten-micron cryosections were sectioned from OCT embedded tissue samples and used for staining. General muscle histopathology was revealed with H&E staining. Dystrophin expression was evaluated by immunofluorescence staining using a monoclonal antibody against the C-terminal domain of the protein (1:20, VP-D505; Vector Laboratories, Burlingame, CA, USA) according to our published

protocol.[74] Laminin was detected using a rabbit polyclonal antibody (1:200, L9393; Sigma, St. Louis, MO, USA) according to our published protocol.[75]

For experiments involving NOD.GFP mice, NSG.GFP mice, Ai14 mice, and Pax7-ZsGreen-Ai14 mice, freshly dissected muscle was immediately fixed in 4% paraformaldehyde overnight at 4°C and then cryo-protected in 30% (w/v) sucrose for 6 h prior to embedding in the OCT medium. GFP, tdTomato, and ZsGreen signals were visualized directly under a fluorescence microscope. For experiments involving NOD.GFP (Figures 2A–2C; Figure S1) and Ai14 mice (Figure 3), Pax7 was detected by immunofluorescence staining with a rabbit polyclonal antibody (1:50, ab187339; Abcam, Cambridge, UK), and PDGFRα was detected by immunofluorescence staining with a rabbit polyclonal antibody (1:100, catalog no. ABIN790499; Antibodies Online, Atlanta, GA, USA). Specifically, 10-μm sections were fixed with 4% paraformaldehyde in PBS for 20 min, then permeabilized in 0.5% Triton X-100 (Sigma, St. Louis, MO, USA) diluted in PBS followed by blocking in 10% fetal bovine serum (Defined; Thermo Fisher Scientific, Waltham, MA, USA), 0.1% Triton X-100 in PBS. The primary antibody was then added at the specified dilution and incubated overnight at 4°C. To reduce background staining, we incubated sections with homemade anti-mouse fragment antigen binding, constant region (FAB-c) diluted 1:1 in PBS prior to blocking.

The secondary antibody (goat anti-rabbit IgG Alexa Fluor 488 or goat anti-mouse IgG Alexa Fluor 594 from Thermo Fisher Scientific, Waltham, MA, USA) was used at 1:100 dilution and was incubated at room temperature for 1 h. Slides were mounted in Citifluor (Citifluor, Hatfield, PA, USA). All images were captured using a Nikon Eclipse E800 fluorescence microscope equipped with a Leica DFC7000T camera and the LAS version 4.9 acquisition software (Leica Biosystems, Wetzlar, Germany).

For morphometric quantification, ×10 images were stitched using the merging and stitching plugins in the NIH ImageJ software (version 1.48b) or the LAS Version 4.9 software (Leica Biosystems, Wetzlar, Germany). All myofibers in the entire cryosection were quantified.

### PCR and Sequencing

Genomic DNA was extracted from OCT embedded samples using genomic DNA prep buffer (50 mM Tris [pH 8.0], 100 mM ethylenediaminetetraacetic acid, 100 mM NaCl, 1% SDS, and Proteinase K 0.5 μg/μL) overnight at 55°C. The solution was flocculated with 6 M NaCl and DNA precipitate by isopropanol. Genomic PCR was performed as previously published.[8] In brief, a forward primer (5′ TTTGTTGATTCTAAAAATCCCATGTTG 3′) in intron 22 and reverse primer (5′ GGACTGAAGAACTTGGAGAAGGA 3′) in intron 23 were used to amplify a fragment spanning exon 23. For PCR, 100 ng of the template DNA was amplified with Q5 High Fidelity polymerase (New England Biolabs, Ipswich, MA, USA) using the following cycling conditions: 92°C for 3 min, 35 cycles at 92°C for 20 s, 60°C or 62.5°C for 20°s, 72°C for 2 min, and final extension at 72°C for 10 min. For nested PCR, 10 μL of the first-round PCR product was mixed with nested forward primer (5′-ATGTCTTAA TAATGTTTCACTGTAGG-3′), nested reverse primer (5′- AAA GGAAGATGGTACAGTGTTAGGG-3′), deoxyribonucleotide triphosphates (dNTPs), and Q5 High Fidelity Taq polymerase. The following cycling conditions were used for nested PCR: 92°C for 3 min, 35 cycles at 92°C for 20 s, 60°C for 20 s, 72°C for 15 s, and final extension at 72°C for 10 min. The PCR product was electrophoresed on a 1% agarose gel. Gel images were captured using a Li-Cor Odyssey Fc imaging system (Li-Cor Biosciences, Lincoln, NE, USA).

Excision of exon 23 and flanking intronic sequence by CRISPR resulted in an ∼470-bp PCR product. This PCR product from nested PCR was gel extracted and blunted using PFUultraII polymerase (Agilent Biosciences, Santa Clara, CA, USA). Blunted PCR products were cloned to a sequencing plasmid pCR using the Zero Blunt pCR cloning kit (Thermo Fisher Scientific, Waltham, MA, USA). Cloned plasmids were transformed to competent *E. coli*. Isolated clones were randomly selected for plasmid preparation. Sanger sequencing was performed using forward and reverse primers in nested PCR. Raw chromatograms were visualized using SnapGene software (version 3.0.3; GSL Biotech).

### gRNA and Cas9 Vector Genome Determination

Genomic DNA extracted from OCT embedded tissue was purified and diluted to 0.5 ng/μL following DNA concentration determination using the Qubit dsDNA high-sensitivity assay kit (Thermo Fisher Scientific, Waltham, MA, USA). Vector genome copy number relative to diploid genomic DNA was determined using a TaqMan PCR assay with TaqMan Universal PCR master mix (Thermo Fisher Scientific, Waltham, MA, USA). Primers and probes for detecting the SaCas9 vector were 5′-CGCACAGAAGATGATCAATGAGATG-3′ (forward primer), 5′-TTCGGATAATCTCTTCAATGCGTTCA-3′ (reverse primer), and 5′-TTGGTCTGCCGGTTTC-3′ (probe). Primers and probes for detecting the gRNA vector were 5′-GAGCGCACCA TCTTCTTCAAG-3′ (forward primer), 5′-TGTCGCCCTCGAACTT CAC-3′ (reverse primer), and 5′-ACGACGGCAACTACA-3′ (probe). Cycle parameters were as follows: 95°C for 10 min followed by 40 cycles of 95°C for 15 s, 60°C for 1 min. The copy number was determined quantitatively by comparing the threshold value with a copy number standard curve derived from known amounts of the *cis* plasmid.

### Statistical Analysis

Data are presented as mean ± SD. Statistical analysis was performed using GraphPad Prism V7 (GraphPad Software, La Jolla, CA, USA). The normality of data distribution was tested with the Shapiro-Wilk normality test. Statistical significance was determined using an unpaired Student's t test with or without a Welch correction depending on the SD. In the case of unequal variance, a Mann-Whitney U test was used. A $p < 0.05$ was considered statistically significant.

## SUPPLEMENTAL INFORMATION

Supplemental Information can be found online at https://doi.org/10.1016/j.ymthe.2019.06.012.

## AUTHOR CONTRIBUTIONS

M.E.N. and D.D. designed the study. M.E.N., R.S., C.H.H., N.B.W., Y.Y., X.P., T.Z., C.A.R., and S.X.D. performed research. T.Z., G.Y., N.N.Y., S.C., K.R.W., and C.A.G. contributed new reagents or analytic tools. M.E.N., R.S., and D.D. analyzed data. M.E.N. and D.D. wrote the paper. M.E.N., C.A.R., R.S., G.Y., K.R.W., T.Z., N.N.Y., S.C., C.A.G., and D.D. edited the paper. M.E.N., G.Y., N.N.Y., S.C., and D.D. secured the funding. All authors discussed the study and approved submission.

## CONFLICTS OF INTEREST

D.D. is a member of the scientific advisory board for Solid Biosciences and equity holder of Solid Biosciences. The Duan lab has received research support unrelated to this project from Solid Biosciences. C.A.G., C.H.H., D.D., and N.B.W. have filed patent applications related to genome editing for Duchenne muscular dystrophy. C.A.G. is an advisor to and receives research support from Sarepta Therapeutics, Inc.

## ACKNOWLEDGMENTS

This work was supported by grants from the NIH (AR-69085 to C.A.G. and D.D.; GM-063732 and GM-117059 to S.C.), Department of Defense (MD15-1-0469 to C.A.G.; MD150133 to D.D., C.A.G., and G.Y.), Jackson Freel DMD Research Fund (to D.D.), Hope for Javier (to D.D. and M.E.N.), and Intramural Research Program of the NIH, NCATS (to N.N.Y. and C.H.H.). M.E.N. is a pre-doctoral fellow supported by Hope for Javier. We thank Dr. Michael Kyba (University of Minnesota) for providing NSG.mdx4cv mice and Pax7-ZsGreen mice. We thank Dr. Jim Wilson (University of Pennsylvania) for providing the AAV9 packaging plasmid. We thank Dr. Weidong Xiao (Temple University) for providing the *cis* plasmid for AAV9.Cre production.

## REFERENCES

1. Mendell, J.R., and Lloyd-Puryear, M. (2013). Report of MDA muscle disease symposium on newborn screening for Duchenne muscular dystrophy. Muscle Nerve *48*, 21–26.
2. Koenig, M., Hoffman, E.P., Bertelson, C.J., Monaco, A.P., Feener, C., and Kunkel, L.M. (1987). Complete cloning of the Duchenne muscular dystrophy (DMD) cDNA and preliminary genomic organization of the DMD gene in normal and affected individuals. Cell *50*, 509–517.
3. Chang, N.C., Chevalier, F.P., and Rudnicki, M.A. (2016). Satellite Cells in Muscular Dystrophy - Lost in Polarity. Trends Mol. Med. *22*, 479–496.
4. Nelson, C.E., Robinson-Hamm, J.N., and Gersbach, C.A. (2017). Genome engineering: a new approach to gene therapy for neuromuscular disorders. Nat. Rev. Neurol. *13*, 647–661.
5. Duan, D. (2018). CRISPR alleviates muscular dystrophy in dogs. Nat. Biomed. Eng. *2*, 795–796.
6. Zhang, Y., Long, C., Bassel-Duby, R., and Olson, E.N. (2018). Myoediting: Toward Prevention of Muscular Dystrophy by Therapeutic Genome Editing. Physiol. Rev. *98*, 1205–1240.
7. Long, C., Amoasii, L., Mireault, A.A., McAnally, J.R., Li, H., Sanchez-Ortiz, E., Bhattacharyya, S., Shelton, J.M., Bassel-Duby, R., and Olson, E.N. (2016). Postnatal genome editing partially restores dystrophin expression in a mouse model of muscular dystrophy. Science *351*, 400–403.
8. Nelson, C.E., Hakim, C.H., Ousterout, D.G., Thakore, P.I., Moreb, E.A., Castellanos Rivera, R.M., Madhavan, S., Pan, X., Ran, F.A., Yan, W.X., et al. (2016). In vivo genome editing improves muscle function in a mouse model of Duchenne muscular dystrophy. Science *351*, 403–407.
9. Tabebordbar, M., Zhu, K., Cheng, J.K.W., Chew, W.L., Widrick, J.J., Yan, W.X., Maesner, C., Wu, E.Y., Xiao, R., Ran, F.A., et al. (2016). In vivo gene editing in dystrophic mouse muscle and muscle stem cells. Science *351*, 407–411.
10. Xu, L., Park, K.H., Zhao, L., Xu, J., El Refaey, M., Gao, Y., Zhu, H., Ma, J., and Han, R. (2016). CRISPR-mediated Genome Editing Restores Dystrophin Expression and Function in mdx Mice. Mol. Ther. *24*, 564–569.
11. Bengtsson, N.E., Hall, J.K., Odom, G.L., Phelps, M.P., Andrus, C.R., Hawkins, R.D., Hauschka, S.D., Chamberlain, J.R., and Chamberlain, J.S. (2017). Muscle-specific CRISPR/Cas9 dystrophin gene editing ameliorates pathophysiology in a mouse model for Duchenne muscular dystrophy. Nat. Commun. *8*, 14454.
12. El Refaey, M., Xu, L., Gao, Y., Canan, B.D., Adesanya, T.M.A., Warner, S.C., Akagi, K., Symer, D.E., Mohler, P.J., Ma, J., et al. (2017). In Vivo Genome Editing Restores Dystrophin Expression and Cardiac Function in Dystrophic Mice. Circ. Res. *121*, 923–929.
13. Hakim, C.H., Wasala, N.B., Nelson, C.E., Wasala, L.P., Yue, Y., Louderman, J.A., Lessa, T.B., Dai, A., Zhang, K., Jenkins, G.J., et al. (2018). AAV CRISPR editing rescues cardiac and muscle function for 18 months in dystrophic mice. JCI Insight *3*, 124297.
14. Amoasii, L., Hildyard, J.C.W., Li, H., Sanchez-Ortiz, E., Mireault, A., Caballero, D., Harron, R., Stathopoulou, T.R., Massey, C., Shelton, J.M., et al. (2018). Gene editing restores dystrophin expression in a canine model of Duchenne muscular dystrophy. Science *362*, 86–91.
15. Wasala, N.B., Hakim, C.H., Chen, S.J., Yang, N.N., and Duan, D. (2019). Questions answered and unanswered by the first CRISPR editing study in a canine model of Duchenne muscular dystrophy. Hum. Gene Ther. *30*, 535–543.
16. Duchêne, B.L., Cherif, K., Iyombe-Engembe, J.P., Guyon, A., Rousseau, J., Ouellet, D.L., Barbeau, X., Lague, P., and Tremblay, J.P. (2018). CRISPR-Induced Deletion with SaCas9 Restores Dystrophin Expression in Dystrophic Models In Vitro and In Vivo. Mol. Ther. *26*, 2604–2616.
17. Iyombe-Engembe, J.P., Ouellet, D.L., Barbeau, X., Rousseau, J., Chapdelaine, P., Lagüe, P., and Tremblay, J.P. (2016). Efficient Restoration of the Dystrophin Gene Reading Frame and Protein Structure in DMD Myoblasts Using the CinDel Method. Mol. Ther. Nucleic Acids *5*, e283.
18. Tremblay, J.P., Iyombe-Engembe, J.P., Duchêne, B., and Ouellet, D.L. (2016). Gene Editing for Duchenne Muscular Dystrophy Using the CRISPR/Cas9 Technology: The Importance of Fine-tuning the Approach. Mol. Ther. *24*, 1888–1889.
19. Duan, D. (2016). Systemic delivery of adeno-associated viral vectors. Curr. Opin. Virol. *21*, 16–25.
20. Duan, D. (2015). Duchenne muscular dystrophy gene therapy in the canine model. Hum. Gene Ther. Clin. Dev. *26*, 57–69.
21. Mendell, J.R., Al-Zaidy, S., Shell, R., Arnold, W.D., Rodino-Klapac, L.R., Prior, T.W., Lowes, L., Alfano, L., Berry, K., Church, K., et al. (2017). Single-dose gene-replacement therapy for spinal muscular atrophy. N. Engl. J. Med. *377*, 1713–1722.
22. Duan, D. (2018). Micro-dystrophin gene therapy goes systemic in Duchenne muscular dystrophy patients. Hum. Gene Ther. *29*, 733–736.
23. Duan, D. (2018). Systemic AAV Micro-dystrophin Gene Therapy for Duchenne Muscular Dystrophy. Mol. Ther. *26*, 2337–2356.
24. Wang, Y.X., and Rudnicki, M.A. (2011). Satellite cells, the engines of muscle repair. Nat. Rev. Mol. Cell Biol. *13*, 127–133.
25. Buckingham, M. (2006). Myogenic progenitor cells and skeletal myogenesis in vertebrates. Curr. Opin. Genet. Dev. *16*, 525–532.
26. Arnett, A.L., Konieczny, P., Ramos, J.N., Hall, J., Odom, G., Yablonka-Reuveni, Z., Chamberlain, J.R., and Chamberlain, J.S. (2014). Adeno-associated viral (AAV) vectors do not efficiently target muscle satellite cells. Mol. Ther. Methods Clin. Dev. *1*, 14038.
27. Carlson, B.M. (1978). A review of muscle transplantation in mammals. Physiol. Bohemoslov. *27*, 387–400.
28. Sloper, J.C., and Partridge, T.A. (1980). Skeletal muscle: regeneration and transplantation studies. Br. Med. Bull. *36*, 153–158.

29. Partridge, T.A., and Sloper, J.C. (1977). A host contribution to the regeneration of muscle grafts. J. Neurol. Sci. *33*, 425–435.

30. Grounds, M.D., and Partridge, T.A. (1983). Isoenzyme studies of whole muscle grafts and movement of muscle precursor cells. Cell Tissue Res. *230*, 677–688.

31. Grounds, M., Partridge, T.A., and Sloper, J.C. (1980). The contribution of exogenous cells to regenerating skeletal muscle: an isoenzyme study of muscle allografts in mice. J. Pathol. *132*, 325–341.

32. Morgan, J.E., Coulton, G.R., and Partridge, T.A. (1987). Muscle precursor cells invade and repopulate freeze-killed muscles. J. Muscle Res. Cell Motil. *8*, 386–396.

33. Shultz, L.D., Lyons, B.L., Burzenski, L.M., Gott, B., Chen, X., Chaleff, S., Kotb, M., Gillies, S.D., King, M., Mangada, J., et al. (2005). Human lymphoid and myeloid cell development in NOD/LtSz-scid IL2R gamma null mice engrafted with mobilized human hemopoietic stem cells. J. Immunol. *174*, 6477–6489.

34. Cao, Y.A., Wagers, A.J., Beilhack, A., Dusich, J., Bachmann, M.H., Negrin, R.S., Weissman, I.L., and Contag, C.H. (2004). Shifting foci of hematopoiesis during reconstitution from single stem cells. Proc. Natl. Acad. Sci. USA *101*, 221–226.

35. Creusot, R.J., Yaghoubi, S.S., Chang, P., Chia, J., Contag, C.H., Gambhir, S.S., and Fathman, C.G. (2009). Lymphoid-tissue-specific homing of bone-marrow-derived dendritic cells. Blood *113*, 6638–6647.

36. Makino, S., Kunimoto, K., Muraoka, Y., Mizushima, Y., Katagiri, K., and Tochino, Y. (1980). Breeding of a non-obese, diabetic strain of mice. Jikken Dobutsu *29*, 1–13.

37. Maykel, J., Liu, J.H., Li, H., Shultz, L.D., Greiner, D.L., and Houghton, J. (2014). NOD-scidIl2rg (tm1Wjl) and NOD-Rag1 (null) Il2rg (tm1Wjl) : a model for stromal cell-tumor cell interaction for human colon cancer. Dig. Dis. Sci. *59*, 1169–1179.

38. Madisen, L., Zwingman, T.A., Sunkin, S.M., Oh, S.W., Zariwala, H.A., Gu, H., Ng, L.L., Palmiter, R.D., Hawrylycz, M.J., Jones, A.R., et al. (2010). A robust and high-throughput Cre reporting and characterization system for the whole mouse brain. Nat. Neurosci. *13*, 133–140.

39. Joe, A.W., Yi, L., Natarajan, A., Le Grand, F., So, L., Wang, J., Rudnicki, M.A., and Rossi, F.M. (2010). Muscle injury activates resident fibro/adipogenic progenitors that facilitate myogenesis. Nat. Cell Biol. *12*, 153–163.

40. Bosnakovski, D., Xu, Z., Li, W., Thet, S., Cleaver, O., Perlingeiro, R.C., and Kyba, M. (2008). Prospective isolation of skeletal muscle stem cells with a Pax7 reporter. Stem Cells *26*, 3194–3204.

41. Mueller, C., Chulay, J.D., Trapnell, B.C., Humphries, M., Carey, B., Sandhaus, R.A., McElvaney, N.G., Messina, L., Tang, Q., Rouhani, F.N., et al. (2013). Human Treg responses allow sustained recombinant adeno-associated virus-mediated transgene expression. J. Clin. Invest. *123*, 5310–5318.

42. Stieger, K., Schroeder, J., Provost, N., Mendes-Madeira, A., Belbellaa, B., Le Meur, G., Weber, M., Deschamps, J.Y., Lorenz, B., Moullier, P., and Rolling, F. (2009). Detection of intact rAAV particles up to 6 years after successful gene transfer in the retina of dogs and primates. Mol. Ther. *17*, 516–523.

43. Schmalbruch, H., and Hellhammer, U. (1976). The number of satellite cells in normal human muscle. Anat. Rec. *185*, 279–287.

44. Schmalbruch, H., and Hellhammer, U. (1977). The number of nuclei in adult rat muscles with special reference to satellite cells. Anat. Rec. *189*, 169–175.

45. Allouh, M.Z., Yablonka-Reuveni, Z., and Rosser, B.W. (2008). Pax7 reveals a greater frequency and concentration of satellite cells at the ends of growing skeletal muscle fibers. J. Histochem. Cytochem. *56*, 77–87.

46. Hawke, T.J., and Garry, D.J. (2001). Myogenic satellite cells: physiology to molecular biology. J. Appl. Physiol. *91*, 534–551.

47. Duan, D., Sharma, P., Yang, J., Yue, Y., Dudus, L., Zhang, Y., Fisher, K.J., and Engelhardt, J.F. (1998). Circular intermediates of recombinant adeno-associated virus have defined structural characteristics responsible for long-term episomal persistence in muscle tissue. J. Virol. *72*, 8568–8577.

48. Schnepp, B.C., Clark, K.R., Klemanski, D.L., Pacak, C.A., and Johnson, P.R. (2003). Genetic fate of recombinant adeno-associated virus vector genomes in muscle. J. Virol. *77*, 3495–3504.

49. Liu, N., Garry, G.A., Li, S., Bezprozvannaya, S., Sanchez-Ortiz, E., Chen, B., Shelton, J.M., Jaichander, P., Bassel-Duby, R., and Olson, E.N. (2017). A Twist2-dependent progenitor cell contributes to adult skeletal muscle. Nat. Cell Biol. *19*, 202–213.

50. Gussoni, E., Soneoka, Y., Strickland, C.D., Buzney, E.A., Khan, M.K., Flint, A.F., Kunkel, L.M., and Mulligan, R.C. (1999). Dystrophin expression in the mdx mouse restored by stem cell transplantation. Nature *401*, 390–394.

51. Birbrair, A., Zhang, T., Wang, Z.M., Messi, M.L., Enikolopov, G.N., Mintz, A., and Delbono, O. (2013). Role of pericytes in skeletal muscle regeneration and fat accumulation. Stem Cells Dev. *22*, 2298–2314.

52. Natarajan, A., Lemos, D.R., and Rossi, F.M.V. (2010). Fibro/adipogenic progenitors: a double-edged sword in skeletal muscle regeneration. Cell Cycle *9*, 2045–2046.

53. Mitchell, K.J., Pannérec, A., Cadot, B., Parlakian, A., Besson, V., Gomes, E.R., Marazzi, G., and Sassoon, D.A. (2010). Identification and characterization of a non-satellite cell muscle resident progenitor during postnatal development. Nat. Cell Biol. *12*, 257–266.

54. Cooper, R.N., Irintchev, A., Di Santo, J.P., Zweyer, M., Morgan, J.E., Partridge, T.A., Butler-Browne, G.S., Mouly, V., and Wernig, A. (2001). A new immunodeficient mouse model for human myoblast transplantation. Hum. Gene Ther. *12*, 823–831.

55. Danko, I., Chapman, V., and Wolff, J.A. (1992). The frequency of revertants in mdx mouse genetic models for Duchenne muscular dystrophy. Pediatr. Res. *32*, 128–131.

56. Partridge, T., and Lu, Q.L. (2008). The enigma of the 'dystrophin revertant' muscle fibre. In Recent Advances in Skeletal Muscle Differentiation, T. Kunihiro and S. Takeda, eds. (Kerala, India: Research Signpost), pp. 93–107.

57. Yokota, T., Lu, Q.L., Morgan, J.E., Davies, K.E., Fisher, R., Takeda, S., and Partridge, T.A. (2006). Expansion of revertant fibers in dystrophic mdx muscles reflects activity of muscle precursor cells and serves as an index of muscle regeneration. J. Cell Sci. *119*, 2679–2687.

58. Lu, Q.L., Morris, G.E., Wilton, S.D., Ly, T., Artem'yeva, O.V., Strong, P., and Partridge, T.A. (2000). Massive idiosyncratic exon skipping corrects the nonsense mutation in dystrophic mouse muscle and produces functional revertant fibers by clonal expansion. J. Cell Biol. *148*, 985–996.

59. Chung, S., Andersson, T., Sonntag, K.C., Björklund, L., Isacson, O., and Kim, K.S. (2002). Analysis of different promoter systems for efficient transgene expression in mouse embryonic stem cell lines. Stem Cells *20*, 139–145.

60. Chakkalakal, J.V., Jones, K.M., Basson, M.A., and Brack, A.S. (2012). The aged niche disrupts muscle stem cell quiescence. Nature *490*, 355–360.

61. Bulfield, G., Siller, W.G., Wight, P.A., and Moore, K.J. (1984). X chromosome-linked muscular dystrophy (mdx) in the mouse. Proc. Natl. Acad. Sci. USA *81*, 1189–1192.

62. Chapman, V.M., Miller, D.R., Armstrong, D., and Caskey, C.T. (1989). Recovery of induced mutations for X chromosome-linked muscular dystrophy in mice. Proc. Natl. Acad. Sci. USA *86*, 1292–1296.

63. Arpke, R.W., Darabi, R., Mader, T.L., Zhang, Y., Toyama, A., Lonetree, C.L., Nash, N., Lowe, D.A., Perlingeiro, R.C., and Kyba, M. (2013). A new immuno-, dystrophin-deficient model, the NSG-mdx(4Cv) mouse, provides evidence for functional improvement following allogeneic satellite cell transplantation. Stem Cells *31*, 1611–1620.

64. Wang, J., Xie, J., Lu, H., Chen, L., Hauck, B., Samulski, R.J., and Xiao, W. (2007). Existence of transient functional double-stranded DNA intermediates during recombinant AAV transduction. Proc. Natl. Acad. Sci. USA *104*, 13104–13109.

65. Wasala, N.B., Lai, Y., Shin, J.-H., Zhao, J., Yue, Y., and Duan, D. (2016). Genomic removal of a therapeutic mini-dystrophin gene from adult mice elicits a Duchenne muscular dystrophy-like phenotype. Hum. Mol. Genet. *25*, 2633–2644.

66. Gao, G., Vandenberghe, L.H., Alvira, M.R., Lu, Y., Calcedo, R., Zhou, X., and Wilson, J.M. (2004). Clades of Adeno-associated viruses are widely disseminated in human tissues. J. Virol. *78*, 6381–6388.

67. Shin, J.-H., Yue, Y., and Duan, D. (2012). Recombinant adeno-associated viral vector production and purification. Methods Mol. Biol. *798*, 267–284.

68. Bruusgaard, J.C., Liestøl, K., Ekmark, M., Kollstad, K., and Gundersen, K. (2003). Number and spatial distribution of nuclei in the muscle fibres of normal mice studied in vivo. J. Physiol. *551*, 467–478.

69. Bruusgaard, J.C., and Gundersen, K. (2008). In vivo time-lapse microscopy reveals no loss of murine myonuclei during weeks of muscle atrophy. J. Clin. Invest. *118*, 1450–1457.

70. Charles, J.P., Cappellari, O., Spence, A.J., Hutchinson, J.R., and Wells, D.J. (2016). Musculoskeletal Geometry, Muscle Architecture and Functional Specialisations of the Mouse Hindlimb. PLoS ONE *11*, e0147669.

71. Heemskerk, A.M., Strijkers, G.J., Vilanova, A., Drost, M.R., and Nicolay, K. (2005). Determination of mouse skeletal muscle architecture using three-dimensional diffusion tensor imaging. Magn. Reson. Med. *53*, 1333–1340.

72. Lieber, R.L. (1997). Muscle fiber length and moment arm coordination during dorsi- and plantarflexion in the mouse hindlimb. Acta Anat. (Basel) *159*, 84–89.

73. Zhang, Y., King, O.D., Rahimov, F., Jones, T.I., Ward, C.W., Kerr, J.P., Liu, N., Emerson, C.P., Jr., Kunkel, L.M., Partridge, T.A., and Wagner, K.R. (2014). Human skeletal muscle xenograft as a new preclinical model for muscle disorders. Hum. Mol. Genet. *23*, 3180–3188.

74. Kodippili, K., Vince, L., Shin, J.H., Yue, Y., Morris, G.E., McIntosh, M.A., and Duan, D. (2014). Characterization of 65 epitope-specific dystrophin monoclonal antibodies in canine and murine models of duchenne muscular dystrophy by immunostaining and western blot. PLoS ONE *9*, e88280.

75. Shin, J.-H., Pan, X., Hakim, C.H., Yang, H.T., Yue, Y., Zhang, K., Terjung, R.L., and Duan, D. (2013). Microdystrophin ameliorates muscular dystrophy in the canine model of duchenne muscular dystrophy. Mol. Ther. *21*, 750–757.